



---

**European Commission  
Research Programme of the Research Fund for Coal and Steel**

**ANGELHY**

**Innovative solutions for design and strengthening of  
telecommunications and transmission lattice towers using large angles  
from high strength steel and hybrid techniques of angles with  
FRP strips**

**WORK PACKAGE 2 – DELIVERABLE 2.1**

**Report about the compression tests on large angle columns in high  
strength steel**

**Coordinator:**

National Technical University of Athens - NTUA, Greece

**Beneficiaries:**

Arcelormittal Belval & Differdange SA - AMBD, Luxembourg

Université de Liège – ULG, Belgium

Cosmote Kinites Tilepikoinonies AE - COSMOTE, Greece

Centre Technique Industriel de la Construction Metallique – CTICM, France

Sika France SAS - Sika France, France

Grant Agreement Number: 753993

26/02/2020

**AUTHORS:**

UNIVERSITE DE LIEGE

Faculty of Applied Sciences, ArGEnCo Department

Quartier Polytech 1, Allée de la Découverte, 9, B52/3, 4000 Liège, Belgium

Authors: Marios-Zois Bezas, Jean-Pierre Jaspart, Jean-François Demonceau, Nicolas Labeye

## **TABLE OF CONTENTS**

<b>1</b>	<b>Introduction</b> .....	<b>4</b>
<b>2</b>	<b>Choice of test specimens</b> .....	<b>4</b>
2.1	Application of Eurocode 3 .....	5
2.2	Preliminary numerical simulations .....	5
2.3	Final selection of the specimens .....	7
2.4	Drawing details .....	8
<b>3</b>	<b>Preparation of the tests – Measurements before and during a test</b> .....	<b>9</b>
3.1	Actual dimensions of the cross-sections .....	10
3.2	Initial Imperfections .....	10
3.3	Material properties .....	14
3.4	Measurements during the test .....	15
<b>4</b>	<b>Results and comparisons</b> .....	<b>17</b>
4.1	Results of the experimental tests.....	17
4.2	Comparison with FEM results .....	18
4.3	Comparison with Eurocode 3.....	20
<b>5</b>	<b>Conclusions</b> .....	<b>21</b>
	<b>References</b> .....	<b>23</b>
	<b>Annex A</b> .....	<b>24</b>
	<b>Annex B</b> .....	<b>28</b>

## 1 Introduction

Task 2.1 of Work Package WP2 of ANGELHY project includes buckling tests on steel columns. Specifically, reference is made to ten (10) buckling tests on columns with large angle profiles from high strength steel. However, the decision has been taken to perform twelve (12) tests instead of ten (10), so as to better cover the influence of some parameters. The experiments have been limited to high strength steel (S460M) only, given the fact that a number of compression tests on angles with lower steel grades have been previously performed by NTUA [1], as well as in Tsinghua University of Beijing [2]. The selection procedure of the specimens, the details about the experimental program such as measurements before and during a tests, as well as the test results, are presented in this report. A comparison of the results obtained through the experiments and numerical simulations, considering relevant imperfections as well as geometrical and material non-linearities, has also been achieved. Finally, a comparison of the test results and the Eurocode predictions has been done. The test campaign has been realised at the “Laboratoire de Mécanique des Matériaux et Structures” at the University of Liège in two different periods due to the late delivery of two specimens.

## 2 Choice of test specimens

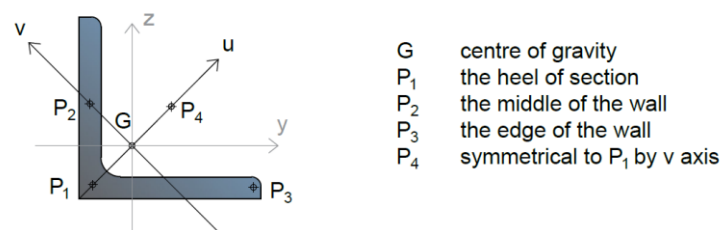
The list of tested profiles, as they are also reported in the proposal document of the project, are summarized in Table 2.1. The mechanical properties have been defined through coupon tests and their results are available in paragraph 3.3.

**Table 2.1: List of tested members cross-sections with their steel grades**

Profile	Grade
L 150x150x18	S460M
L 200x200x16	S460M

For each profile identified in Table 2.1, six column tests have been performed by varying the following parameters:

- The member length. Four possible lengths per profile 2.5, 3.0, 3.5, 4.0 m, resulting in different global slenderness.
- The eccentricity of the applied load. There are 5 points of interest (G, P<sub>1</sub>, P<sub>2</sub>, P<sub>3</sub>, P<sub>4</sub>) as far as the position of the applying load (see Figure 2.1) is concerned.



**Figure 2.1: Possible positions of the applied load**

Before the test specimens may be designed, it is necessary to recall the principal limitations of the used testing machine (Amsler 500):

- maximum length of the tested members: 5,0 m;
- maximum applying load: 500 t (=5000 kN).

Two parameters are considered to select the test specimens. The first one is the failure load according to Eurocode 3 and to preliminary numerical simulations. The second one is the failure mode of the column, obtained through those numerical simulations.

## 2.1 Application of Eurocode 3

According to EN1993-1-1 [3] the first profile (L 150x150x18) is classified as Class 1 and the second one (L 200x200x16) as Class 4. The procedure of EN1993-1-5 [4] has been followed to evaluate the effective cross-section of the Class 4 profile and a reduction factor for the area equal to  $\beta=0,852$  has been obtained.

Table 2.2 shows the results of the application of EN1993-1-1 (buckling resistance) for each profile and for different lengths in the case where no eccentricity is assumed (centroid load). This assumption of “no eccentricity” is made so as to derive the highest possible nominal resistance and compare it to the capacity of the testing machine. Based on the results of the table, for each case the failure mode is a flexural buckling about v axis except case 5, which is a flexural-torsional (see Figure 2.1 for the definition of the axis).

**Table 2.2: Application of EN 1993-1-1**

No	Profile	Area		Buckling length	Minimum elastic critical load /mode		Reference slenderness	Reduction factor	Axial resistance by EC3
		A [cm <sup>2</sup> ]	$\beta$ [-]	L <sub>crit</sub> [mm]	N <sub>cr</sub> [kN]	mode	$\bar{\lambda}$ [-]	$\chi$ [-]	N <sub>b,Rd</sub> [kN]
1	L150x150x18	51,00	1,00	2500	1427,84	F	1,282	0,4356	1022,43
2	L150x150x18	51,00	1,00	3000	991,55	F	1,539	0,3284	770,88
3	L150x150x18	51,00	1,00	3500	728,49	F	1,795	0,2533	594,50
4	L150x150x18	51,00	1,00	4000	557,75	F	2,052	0,2002	469,88
5	L200x200x16	61,75	0,85	2500	3076,74	FT	0,887	0,6696	1620,50
6	L200x200x16	61,75	0,85	3000	2201,21	F	1,049	0,5666	1371,12
7	L200x200x16	61,75	0,85	3500	1617,21	F	1,223	0,4656	1126,90
8	L200x200x16	61,75	0,85	4000	1238,18	F	1,398	0,3825	925,74

\*F=flexural mode, FT=flexural torsional mode

## 2.2 Preliminary numerical simulations

As previously mentioned, the choice of the test specimens was also based on numerical simulations considering relevant imperfections as well as geometrical and material non-linearities. Specifically, for each preliminary analysis (GMNIA), one considers:

- an initial bow imperfection of magnitude equal to L(mm)/1000, with a deformation shape similar to the first instability mode of the member;
- residual stresses which result from hot-rolling; the assumed pattern which is shown in Figure 2.2 has been used in many scientific papers [5] and is a common one for Eurocode’s studies too;
- an elastic-perfectly plastic material law with yield stress equal to 460 N/mm<sup>2</sup> and modulus of elasticity 210000 N/mm<sup>2</sup> (see Figure 2.3).

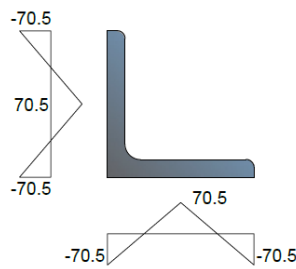


Figure 2.2: Assumed distribution of residual stresses

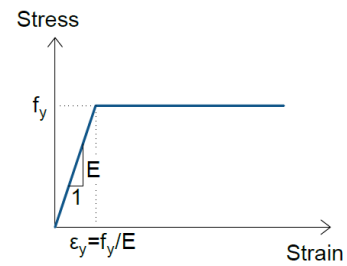


Figure 2.3: Stress-strain curve used for preliminary numerical studies

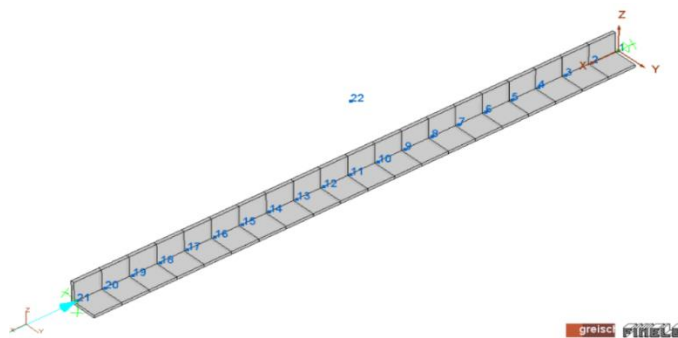


Figure 2.4: Global view of the numerical model used for the preliminary analyses of the test specimens

The numerical analyses of the test specimens were performed with FINELG [6] non-linear finite element software, using beam elements (see Figure 2.4). Only the column has been simulated while the end plates at the extremities (end plates actually welded at the ends of the tested specimens) have been considered indirectly. The columns are assumed as pin-end members with free rotations at their extremities, except the rotation which leads to torsion that is blocked. All the other DOF at the extremities are blocked, except  $u_x$  of node 21. The FEM nodes are located at the centre of gravity of the angle cross-section, while the “fictitious” node 22 is numerically used only for the orientation of the beam elements.

The results from all the non-linear analyses are summarized in Table 2.3 and Table 2.4. Both tables include results with and without eccentricities according to the five possible load application points shown in Figure 2.1. Furthermore, both tables report the estimated failure mode that is – as already referred – one of the parameters to select the test specimens.

Table 2.3: Ultimate axial load [kN] & failure mode for different eccentricities for L150x150x18

No	Profile	Length $L_{tot}$ [mm]	Eccentricities [mm]				
			G	P <sub>1</sub>	P <sub>2</sub>	P <sub>3</sub>	P <sub>4</sub>
			$e_{0u}=0,00$ $e_{0v}=0,00$	$e_{1u}=-48,74$ $e_{1v}=0,00$	$e_{2u}=0,00$ $e_{2v}=48,74$	$e_{3u}=48,74$ $e_{3v}=-97,48$	$e_{4u}=48,74$ $e_{4v}=0,00$
1	L 150x150x18	2500	1178,44 <i>Flexural</i>	508,46 <i>Flexural</i>	794,98 <i>Flexural</i>	376,96 <i>Flexural</i>	480,59 <i>Flexural</i>
2	L 150x150x18	3000	871,90 <i>Flexural</i>	434,44 <i>Flexural</i>	689,64 <i>Flexural</i>	333,90 <i>Flexural</i>	409,33 <i>Flexural</i>
3	L 150x150x18	3500	660,70 <i>Flexural</i>	372,01 <i>Flexural</i>	578,62 <i>Flexural</i>	296,34 <i>Flexural</i>	350,32 <i>Flexural</i>

4	L 150x150x18	4000	515,22	320,09	475,81	263,09	301,19
			<i>Flexural</i>	<i>Flexural</i>	<i>Flexural</i>	<i>Flexural</i>	<i>Flexural</i>

Table 2.4: Ultimate axial load [kN] & failure mode for different eccentricities for L200x200x16

No	Profile	Length $L_{tot}$ [mm]	Eccentricities [mm]				
			G	P <sub>1</sub>	P <sub>2</sub>	P <sub>3</sub>	P <sub>4</sub>
			$e_{0u}=0,00$ $e_{0v}=0,00$	$e_{1u}=-66,64$ $e_{1v}=0,00$	$e_{2u}=0,00$ $e_{2v}=-66,64$	$e_{3u}=66,64$ $e_{3v}=-133,28$	$e_{4u}=66,64$ $e_{4v}=0,00$
1	L 200x200x16	2500	2278,22	742,94	1143,18	521,77	731,92
			<i>Flexural - Torsional</i>	<i>Flexural</i>	<i>Flexural - Torsional</i>	<i>Flexural - Torsional</i>	<i>Flexural - Torsional</i>
2	L 200x200x16	3000	1690,99	671,40	1029,11	477,42	639,64
			<i>Flexural</i>	<i>Flexural</i>	<i>Flexural - Torsional</i>	<i>Flexural - Torsional</i>	<i>Flexural</i>
3	L 200x200x16	3500	1354,46	597,50	936,95	437,67	566,50
			<i>Flexural</i>	<i>Flexural</i>	<i>Flexural - Torsional</i>	<i>Flexural - Torsional</i>	<i>Flexural</i>
4	L 200x200x16	4000	1084,52	532,90	844,14	398,71	501,78
			<i>Flexural</i>	<i>Flexural</i>	<i>Flexural - Torsional</i>	<i>Flexural - Torsional</i>	<i>Flexural</i>

### 2.3 Final selection of the specimens

The decision has been taken to perform the tests with three different lengths per profile and two eccentricities for each length. The load application points which have been adopted are shown in Figure 2.5. From the five points illustrated in Figure 2.1, the following ones have been selected:

- the centre of gravity, which is a very important node as it corresponds to pure compression in the angle;
- the middle of the wall, which is the most usual connection point for angles in structures (position of the connecting bolt).

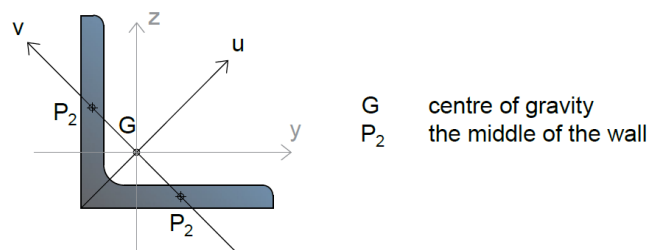


Figure 2.5: Final position of applicable load

The final parameters of the specimens are summarized in Table 2.5. The name of each specimen consists of two numbers Sp## (e.g. Sp13):

- the first number indicates the profile: 1 for L150x150x18 and 2 for 200x200x16;
- the second one is the serial number of the specimen (1 to 6 per profile).

Table 2.5: Final parameters about the specimens

ID of Specimen	Profile	Steel grade	Length [mm]	Eccentricity [mm]	Estimate (GMNIA) failure load [kN]
Sp11	L 150x150x18	S460	2500	0,00	1178,44
Sp12	L 150x150x18	S460	2500	$e_v=48,74$	794,98
Sp13	L 150x150x18	S460	3000	0,00	871,90
Sp14	L 150x150x18	S460	3000	$e_v=48,74$	672,83
Sp15	L 150x150x18	S460	3500	0,00	660,70
Sp16	L 150x150x18	S460	3500	$e_v=48,74$	578,62
Sp21	L 200x200x16	S460	3000	0,00	1690,99
Sp22	L 200x200x16	S460	3000	$e_v=66,64$	1029,11
Sp23	L 200x200x16	S460	3500	0,00	1354,46
Sp24	L 200x200x16	S460	3500	$e_v=66,64$	936,95
Sp25	L 200x200x16	S460	4000	0,00	1084,52
Sp26	L 200x200x16	S460	4000	$e_v=66,64$	844,14

## 2.4 Drawing details

For all tests, constant dimensions have been selected for the end plates welded at the extremities of the angles members, in order to simplify the placement procedure of the specimen in the test rig. The advantage of this decision is that the bolts and the position of the applied load in the test rig are the same for all the tests and the actual eccentricity depends on the position of the profile on the end plates. As a result, the preparation time of the experiments has been significantly reduced. The steel grade of the end plates is S355 and not S460 as for the profiles. The following figures show the details of these end plates on which the specimens have been welded.

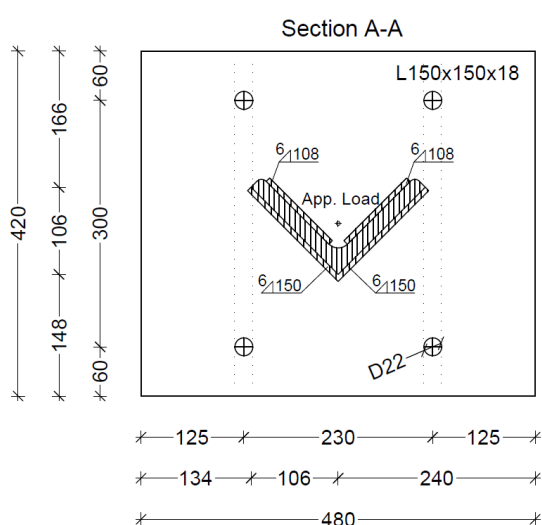


Figure 2.6: Detail of end plate in case of centrally load specimen

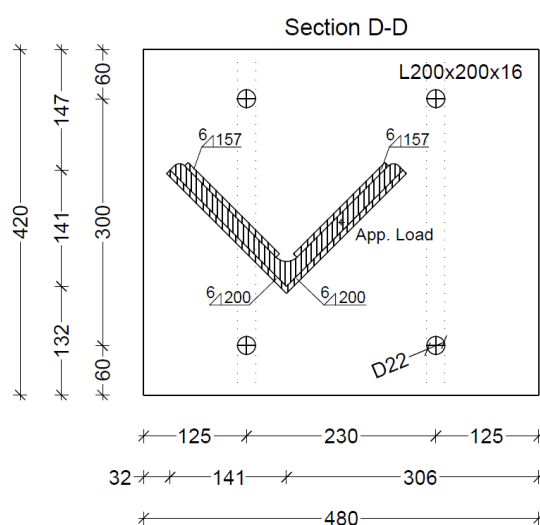


Figure 2.7: Detail of end plate in case of eccentrically load specimen



The welds have been designed according to EN1993 – 1 – 8 [7]. The welding lengths are shown in Figure 2.6 and Figure 2.7 and include all the straight sides of the cross-sections. For all the specimens, the minimum required weld thickness is 6 mm, except for specimens Sp11 and Sp21 which require a minimum thickness of 8 mm. The full drawings are reported in Annex A.

### 3 Preparation of the tests – Measurements before and during a test

Before the experiments, a preparation of the specimens itself and the test rig is necessary. First, the actual dimensions, as well as the initial imperfections of the specimens have been measured. At the same time, coupon tests have been performed in order to evaluate the actual strain-stress curve of the material. The measurements to be done during an experimental test are reported in paragraph 3.4. A sketch of the testing machine is presented in Figure 3.1.

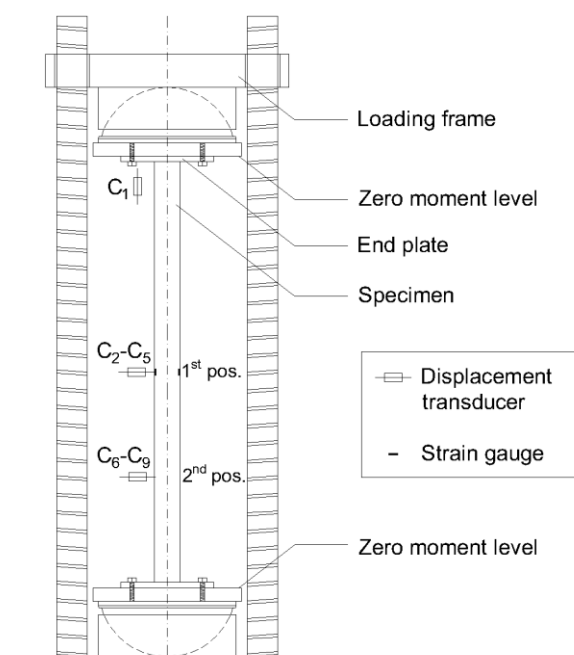


Figure 3.1: Sketch of Amsler 500 test machine

Four strain gauges ( $I_1$  to  $I_4$ ) have been placed at the mid-height cross-section of each column as shown in Figure 3.2, in order to check the local yielding. The strain gauges have been placed as closer as possible to the edge of the cross-section, taken into account the curvature of the edges.

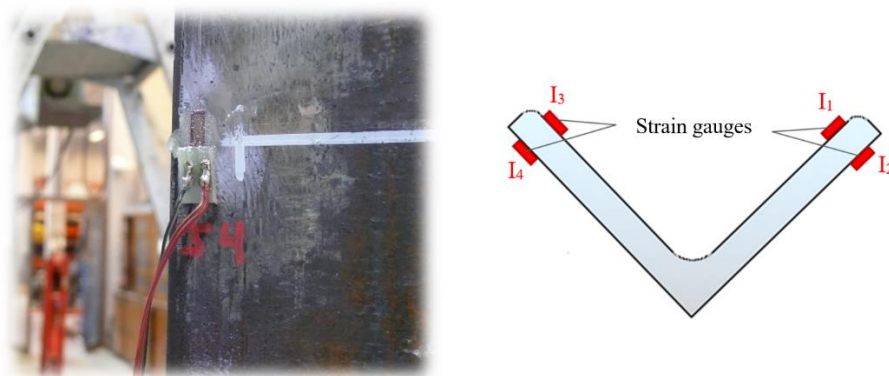


Figure 3.2: Position and numbering of strain gauges at the mid-height cross-section

### 3.1 Actual dimensions of the cross-sections

The actual geometrical dimensions of each angle section – the width ( $b_i$ ) and the thickness ( $t_i$ ) of each leg – have been measured at 3 points along the member length: 1/4, 1/2 and 3/4 of the total length ( $L$ ). The mean values of the measurements are reported in Table 3.1 below.

Table 3.1: Measurements of the actual dimensions of the cross-sections

ID of Specimen	Length [mm]	$b_1$ [mm]	$b_2$ [mm]	$t_1$ [mm]	$t_2$ [mm]	$b_m$ [mm]	$t_m$ [mm]
Sp11	2500	149,97	150,09	18,16	18,14	150,03	18,15
Sp12	2500	150,07	150,12	18,18	18,04	150,10	18,11
Sp13	3000	150,11	149,92	18,04	18,16	150,02	18,10
Sp14	3000	150,09	150,10	18,04	18,17	150,09	18,11
Sp15	3500	150,07	150,11	18,17	18,07	150,09	18,12
Sp16	3500	150,11	149,95	18,16	18,19	150,03	18,17
Sp21	3000	200,31	200,41	16,32	16,34	200,36	16,33
Sp22	3000	200,36	200,39	16,39	16,29	200,37	16,34
Sp23	3500	200,25	199,92	16,32	16,28	200,08	16,30
Sp24	3500	200,05	200,01	16,42	16,10	200,03	16,26
Sp25	4000	199,96	200,27	16,33	16,35	200,12	16,34
Sp26	4000	200,06	200,39	16,32	16,31	200,22	16,32

$b_i=1/3(b_i^{L1/4}+b_i^{L1/2}+b_i^{L3/4})$  ( $i=1,2$ ) ;  $t_i=1/3(t_i^{L1/4}+t_i^{L1/2}+t_i^{L3/4})$  ( $i=1,2$ ) ;  $b_m=(b_1+b_2)/2$  ;  $t_m=(t_1+t_2)/2$

### 3.2 Initial Imperfections

Two measurements ( $M_1$  &  $M_2$ ) on each external face and along the column length have been performed so as to evaluate the initial deformation of the specimens. Figure 3.3 shows the orientation of the specimen on the set-up during the measurement on each face, while Figure 3.4 shows the details of the set-up configuration. Due to the end plates and the measurement system itself, it wasn't possible to take measurements quite close to the ends of the specimens. As a result, all the measurements start 140 mm after the top end plate and finish 140 mm before the bottom one. A measurement has been taken every 50 mm along the column. It is quite reasonably assumed that the columns close to the end plates (140 mm) are straight.

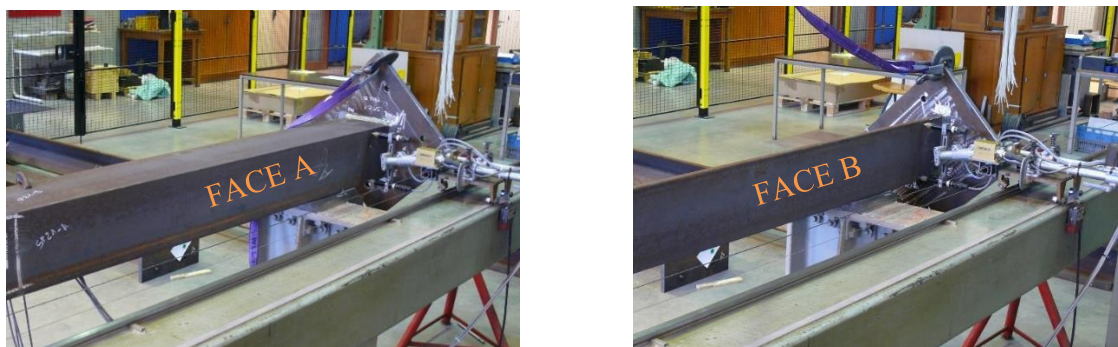


Figure 3.3: Position of the specimens during the initial imperfections measurements (measurement on face A on the left and on face B on the right)

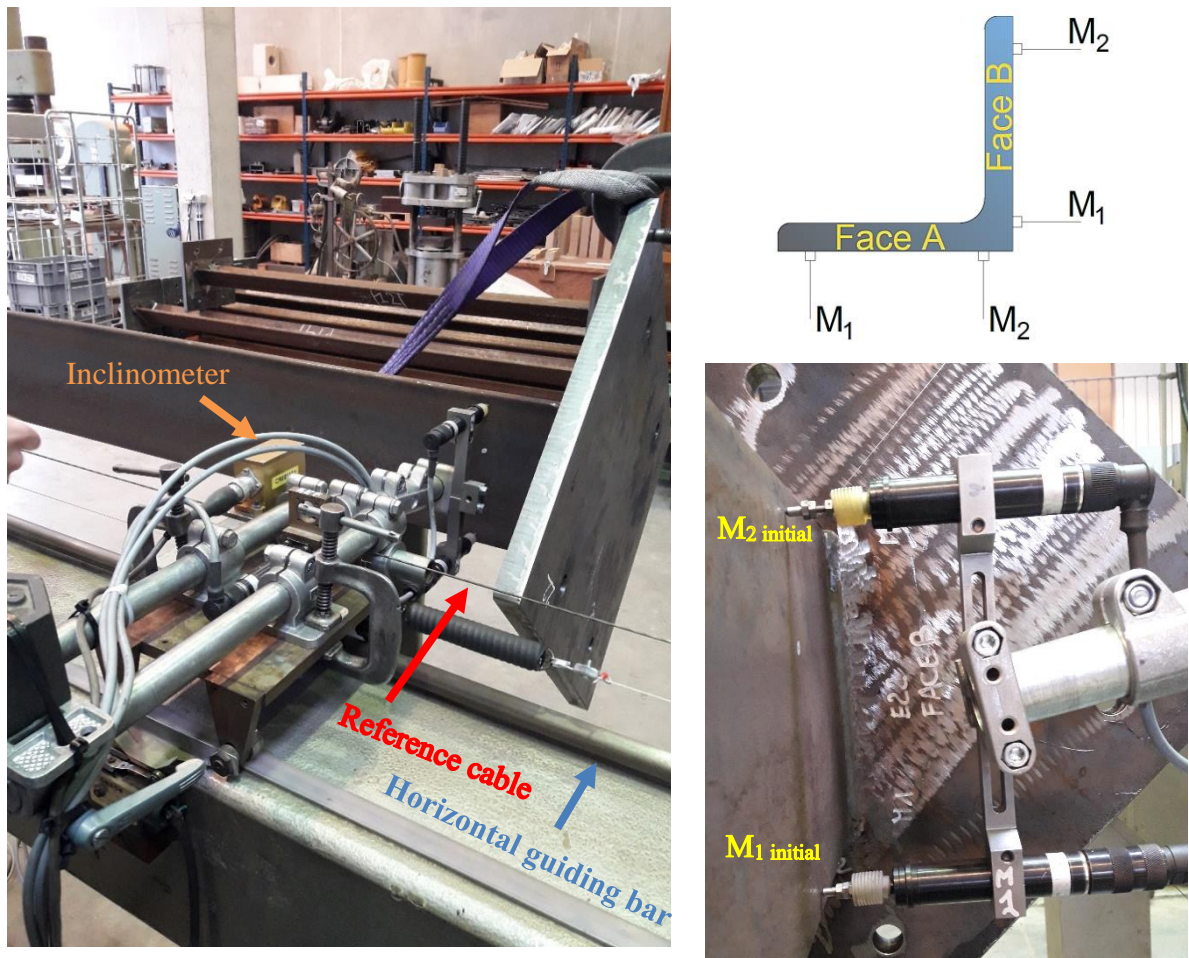


Figure 3.4: Measurement system for geometrical imperfections (left), detail and position of the displacement transducers (right)

The measurements of the initial imperfections are reported in graphs in Annex B for each specimen. However, an explanation about the results and symbols is presented below for specimen 15. Figure 3.5 shows the initial measurements on face B for specimen 15, as they are obtained through the set-up system. For all the graphs, the horizontal axis represents the length of the column (for Sp15, L equals 3500mm).

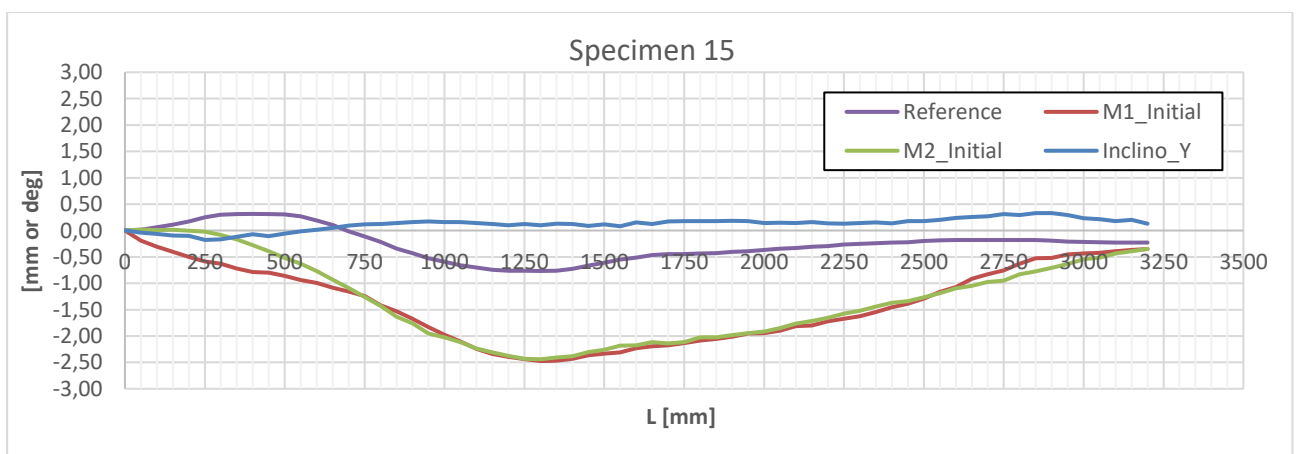


Figure 3.5: Initial measurements for specimen 15 on face B

As the chariot supporting the inclinometer was moving onto a horizontal guiding bar, a small rotation of the metric system was created. In addition, the column wasn't perfectly parallel to the set-up. For those reasons, the first correction to achieve concerns the non-parallelism and the rotation of the metric system; it is based always on the position of the reference cable (curves M1 and M2 on Figure 3.6), using the following formulae (eq.1 to eq.4):

- Profiles 150x150x18, both faces:

$$M_1 = M1\_Inital + 0,7 \cdot Inclino\_Y - (Reference - 1,3 \cdot Inclino\_Y) \quad (\text{eq. 1})$$

$$M_2 = M2\_Inital + 1,5 \cdot Inclino\_Y - (Reference - 1,3 \cdot Inclino\_Y) \quad (\text{eq. 2})$$

- Profiles 200x200x16, both faces:

$$M_1 = M1\_Inital + 0,7 \cdot Inclino\_Y - (Reference - 1,3 \cdot Inclino\_Y) \quad (\text{eq. 3})$$

$$M_2 = M2\_Inital + 2,4 \cdot Inclino\_Y - (Reference - 1,3 \cdot Inclino\_Y) \quad (\text{eq. 4})$$

Then, a second correction has been done in order to have zero imperfection at the extremities of the column (curves M1C(B)\* and M2C(B)\* on Figure 3.6).

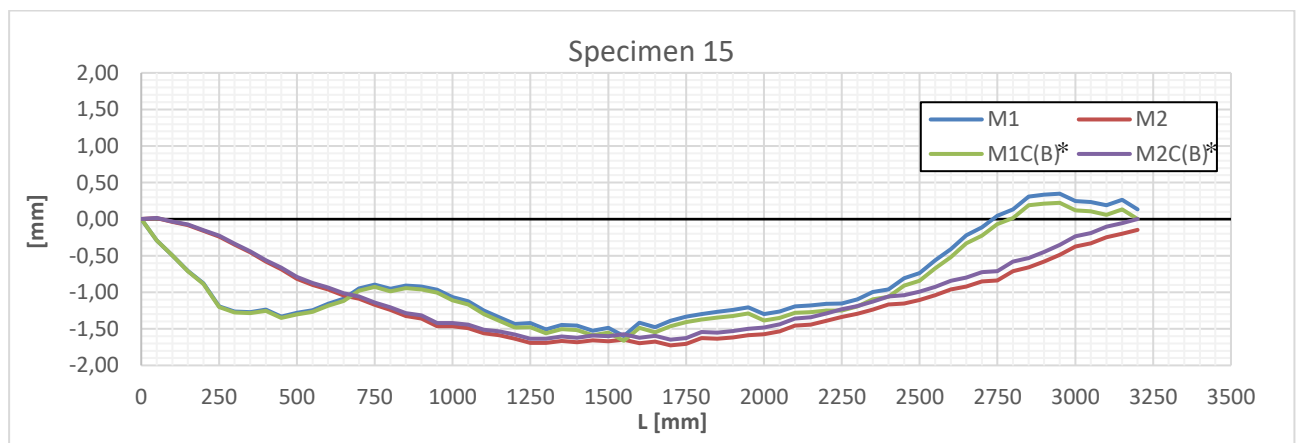


Figure 3.6: Corrected measurements for specimen 15 on face B

Finally, a horizontal movement of the curve has been achieved in such a way that the first measurement lies at 140mm. The same procedure has been followed for face A and the final imperfection curves are presented in Figure 3.7. As already mentioned, at the extremities of the column it is assumed that the member is straight. Figure 3.4 shows the definition of the numbers 1 and 2 used on the graphs:

- M1C(A) is the M1 final corrected measurement on face A for specimen i;
- M2C(A) is the M2 final corrected measurement on face A for specimen i;
- M1C(B) is the M1 final corrected measurement on face B for specimen i;
- M2C(B) is the M2 final corrected measurement on face B for specimen i;
- L is the total length of specimen i.

For specimens Sp11 and Sp24, a laser set-up (Figure 3.8) has been used for the evaluation of the initial geometrical imperfections (tests performed later than the others, for organisational reasons). The testing procedure and the measurements are exactly the same than for the previous tests, except that laser measures are here used. The derivation of the final imperfections is similar, now using however the following equations (eq.5 to eq.8):

- Profiles 150x150x18, both faces:

$$M_1 = M1\_Inital - 1,1 \cdot Inclino\_Y - (Reference + Inclino\_Y) \quad (\text{eq. 5})$$



$$M_2 = M2\_Inital + 0,9 \cdot Inclino\_Y - (Reference + Inclino\_Y) \quad (\text{eq. 6})$$

- Profiles 200x200x16, both faces:

$$M_1 = M1\_Inital - 1,1 \cdot Inclino\_Y - (Reference + Inclino\_Y) \quad (\text{eq. 7})$$

$$M_2 = M2\_Inital + 1,7 \cdot Inclino\_Y - (Reference + Inclino\_Y) \quad (\text{eq. 8})$$

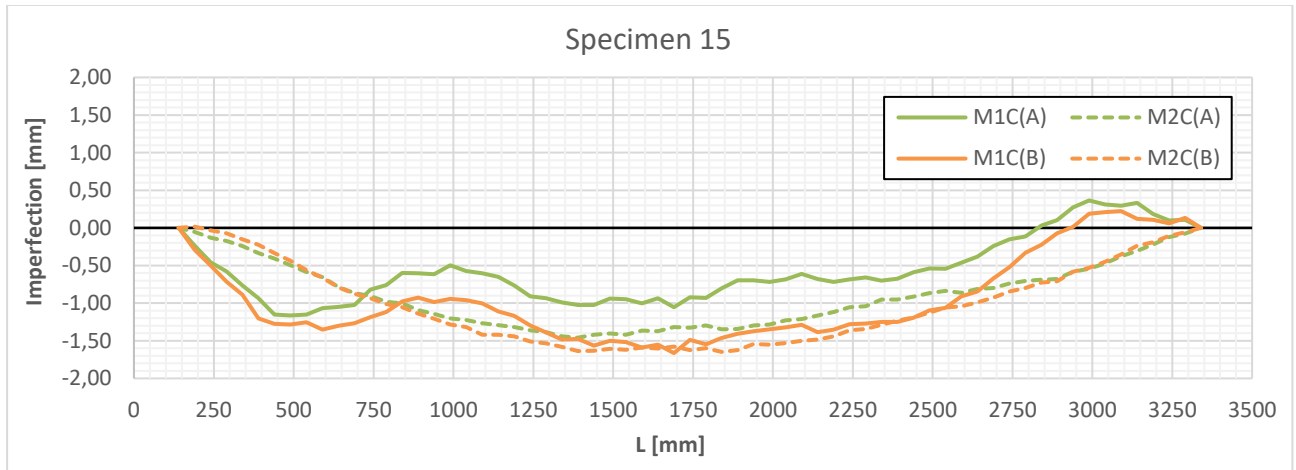


Figure 3.7: Initial imperfections of both faces along specimen 15

The same measurement system with the laser transducers will be also used for the experimental campaign concerning closely spaced built-up members made of angles, which is part of ANGELHY WP3.

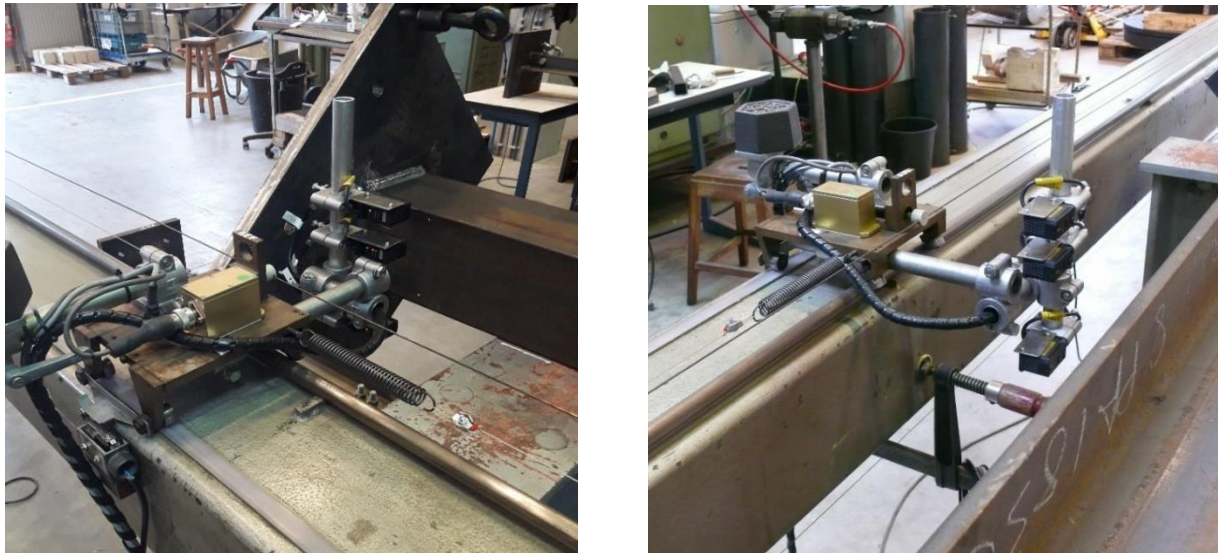


Figure 3.8: Configurations of the laser measurement system

An accurate comparison between the actual measured imperfections of the specimens and those assumed in the Eurocode is quite difficult to do. European norms [8],[9] and [10], prescribe an initial bow imperfection of magnitude equal to  $L[\text{mm}]/1000$  and a deformation shape similar to the first member instability mode, while in reality the shape is more complex. For this reason, only a rough comparison could be done at this level (see Table 3.2), by taking into account the maximum value [M1C(A), M2C(A), M1C(B), M2C(B)] and assumed that it is the same in both faces:

$$|Max|_{imperf} = \max\{M1C(A), M2C(A), M1C(B), M2C(B)\} \cdot \sqrt{2} \quad (\text{eq. 9})$$

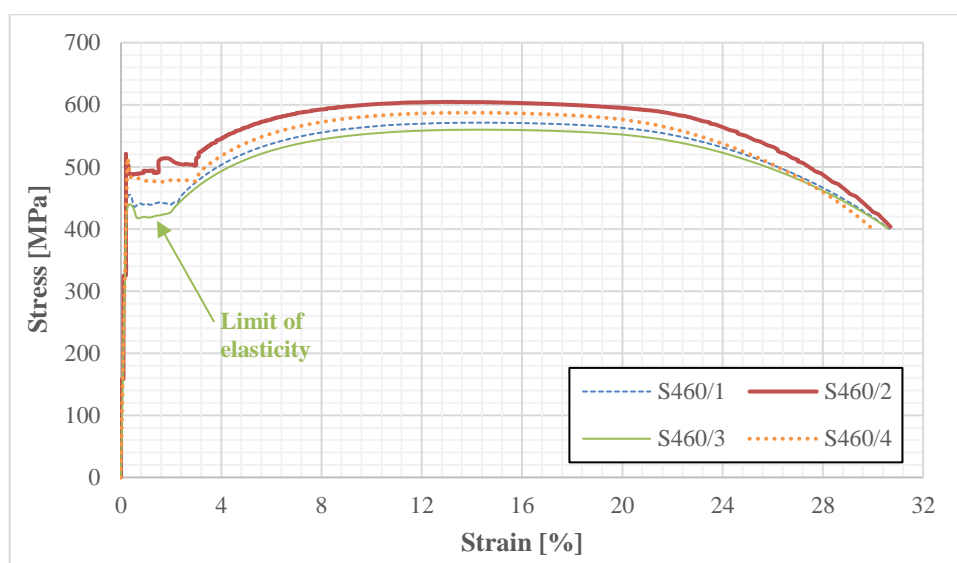
Then, it can be concluded that measured imperfections were smaller for all specimens than the geometrical tolerances prescribed in European regulations and so the specimens are quite straight.

**Table 3.2: Maximum values of the actual initial imperfections of the specimens compared with EN predictions**

ID of Specimen	L/1000 [mm]	Max  <sub>imperf</sub> [mm]	Difference [%]
Sp11	2,5	0,4	-84
Sp12	2,5	1,2	-52
Sp13	3,0	1,3	-57
Sp14	3,0	0,8	-72
Sp15	3,5	2,4	-33
Sp16	3,5	3,0	-15
Sp21	3,0	1,6	-47
Sp22	3,0	2,7	-11
Sp23	3,5	1,7	-50
Sp24	3,5	2,8	-21
Sp25	4,0	1,5	-62
Sp26	4,0	1,8	-55

### 3.3 Material properties

Coupon tests have been performed in accordance with ISO 6892-1:2016 [11] and ISO 377:1997 [12]. Figure 3.9 shows the strain – stress curves obtained from those tensile tests and Table 3.3 the characteristic values of the mechanical properties. For the validation of the tests, the “limit of elasticity” (“actual” yield stress) corresponds to the value of the plateau in the  $\sigma$ - $\epsilon$  material curves. Specimens Sp11 and Sp24 have their own strain-stress curve as they have been fabricated at a different time from the others.



**Figure 3.9: Stain-stress curves from the coupon tests**

Table 3.3: Coupon test's results

No	ID of material	E [MPa]	Yielding stress $f_y$ (ReH) [MPa]	Limit of Elasticity [Mpa]	Ultimate stress $f_{ult}$ [MPa]	Characterized specimens
1	S 460/1	203155	455,2	425,8	572,50	Sp12, Sp13, Sp14, Sp15, Sp16
2	S 460/2	208947	520,7	487,6	604,64	Sp21, Sp22, Sp23, Sp25, Sp26
3	S 460/3	197317	439,7	417,2	560,87	Sp11
4	S 460/4	203797	514,5	472,6	587,21	Sp24

### 3.4 Measurements during the test

During the tests, the following displacements illustrated in Figure 3.10 were measured:

- the vertical displacement  $C_1$ ;
- four horizontal displacements  $C_2, C_3, C_4$  and  $C_5$  at the mid cross-section (1<sup>st</sup> position);
- four horizontal displacements  $C_6, C_7, C_8$  and  $C_9$  at the lower cross-section (2<sup>nd</sup> position).

All the displacement transducers have been placed 30 mm from the edges/corner of all cross-sections and profiles. The configuration of the test rig allowing to record those displacements, is shown in Figure 3.11.

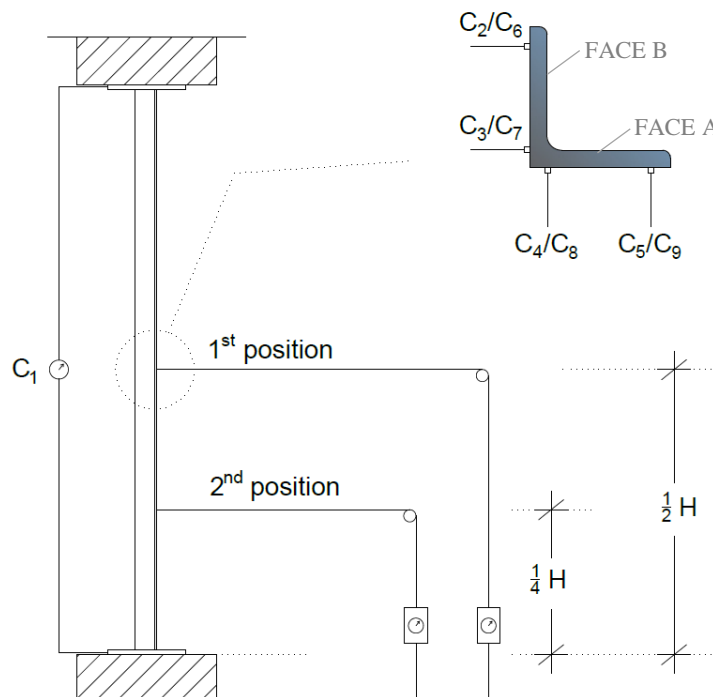


Figure 3.10: Measurements during a test (H is the height of the specimen)

The displacements of the corner of the angle (O point) as well as the torsional rotation of the cross-section, have been evaluated using the following formulae (for the definition of the axes and symbols, see Figure 3.12 left):



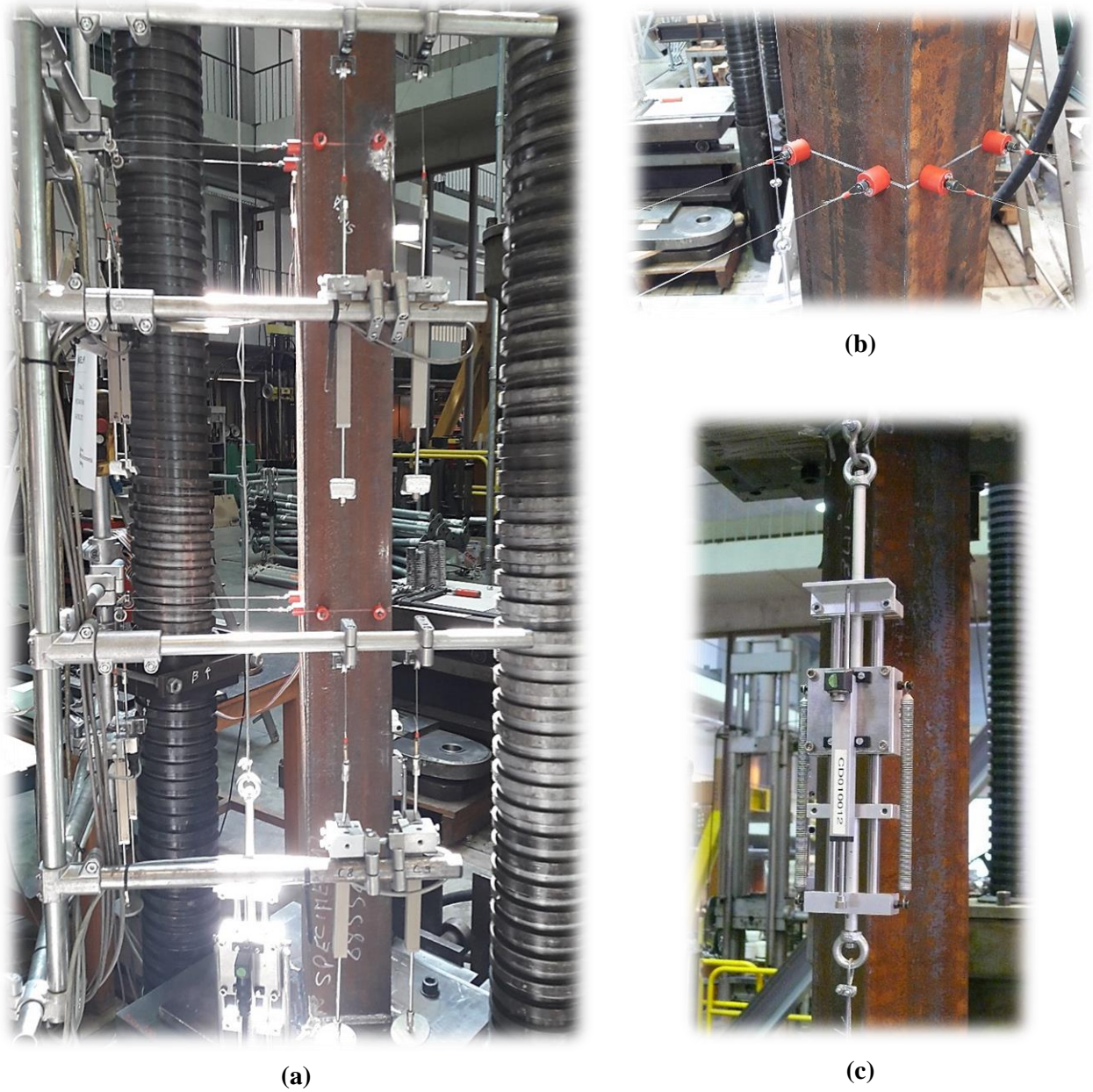


Figure 3.11: (a) General view of test rig with the measurement devices, (b) Connection points of displacement transducers on the cross-section and (c) Vertical displacement transducer

$$y_0 = C_3 + 30 \cdot \frac{C_3 - C_2}{d} \text{ [mm]} \quad (\text{eq.10})$$

$$z_0 = C_4 - 30 \cdot \frac{C_5 - C_4}{d} \text{ [mm]} \quad (\text{eq.11})$$

$$\theta_A = 1000 \cdot \text{atan} \left( \frac{C_3 - C_2}{d} \right) \text{ [mrad]} \quad (\text{eq.12})$$

$$\theta_B = 1000 \cdot \text{atan} \left( \frac{C_5 - C_4}{d} \right) \text{ [mrad]} \quad (\text{eq.13})$$

$$\theta_{\text{mean}} = \left( \frac{\theta_A + \theta_B}{2} \right) \text{ [mrad]} \quad (\text{eq.14})$$

$$\Delta\varphi = \theta_B - \theta_A \text{ [mrad]} \quad (\text{eq.15})$$



where  $d=90/140$  [mm] for L150x150x18/L200x200x16. The formulae are given for the middle cross-section. However, they may also be used for the lower one, by replacing  $C_2$ ,  $C_3$ ,  $C_4$  and  $C_5$  by  $C_6$ ,  $C_7$ ,  $C_8$  and  $C_9$  respectively.

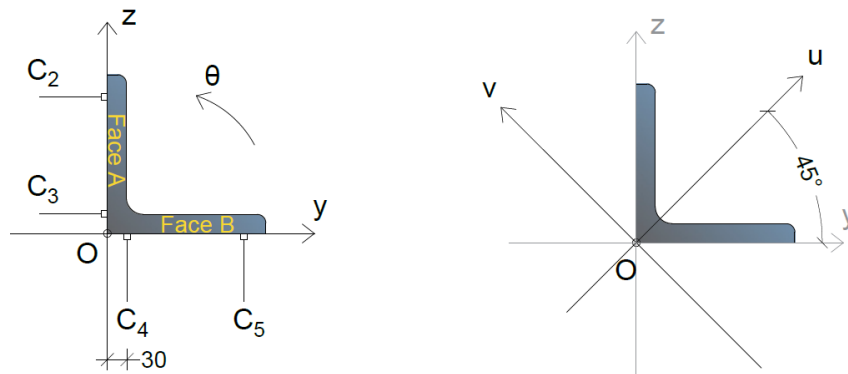


Figure 3.12: Definition of axis and symbols for measurements

To transform the displacements from the  $y$ - $z$  axes to the  $u$ - $v$  principal axes (see Figure 3.12 right), the following equations have been used, for an angle equal to  $45^\circ$ .

$$u_i = y_i \cos\theta + z_i \sin\theta = (y_i + z_i) \cdot \frac{\sqrt{2}}{2} \quad (\text{eq.16})$$

$$v_i = z_i \cos\theta - y_i \sin\theta = (z_i - y_i) \cdot \frac{\sqrt{2}}{2} \quad (\text{eq.17})$$

## 4 Results and comparisons

The results of the tests are presented below through graphs and tables. Numerical simulations of the tests with FINELG have been performed, by taking into account the actual dimensions, length, imperfections and material properties. Finally, a comparison between the ultimate resistance obtained by the tests and through EN1993-1-1 predictions has also been achieved for centrally loaded columns.

### 4.1 Results of the experimental tests

Figure 4.1 and Figure 4.2 show the axial displacement versus the applied load for profiles L150x150x18 and L200x200x16 respectively. Annex B includes all the measurements (inclinometer, initial imperfections, strains and deflections) for each specimen. Due to the existing deformations between specimen's end plates and machine's plates, some deformations occurred at low levels of loading, until a full contact of the plates was reached. To delete these unwanted displacements, a small loading – unloading cycle was performed in the elastic range. By using the slope of the unloading branch, the curves were corrected and illustrated in the following graphs.

Figure 4.1 and Figure 4.2 indicate that the results obtained for the tests are in line with the physical expectations (for instance, the influence of the member length and of the eccentricity on the member stiffness and resistance properties look conform to what was physically expected). This seems a priori to validate the initial selection of the different parameters in test campaign.

It has also been observed that for all specimens without loading eccentricity a pure flexural buckling occurred while specimens with load eccentricity reached failure with a flexural-torsional buckling deformations. More precisely, in the second case, one sees that the cross-section at mid-height of the column starts to twist at low levels of loading and then deforms laterally until failure when flexural buckling develops. Local buckling was not observed in any specimen despite the fact that L 200x200x16 angles are recognised as Class 4 according to Eurocode 3 Part 1-1.

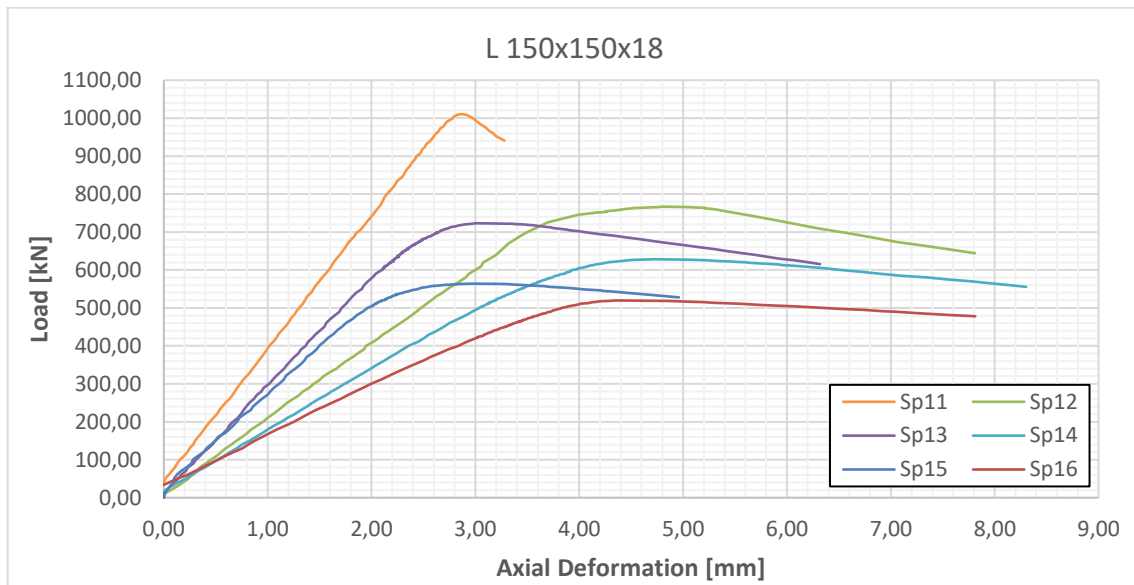


Figure 4.1: Load vs axial deformation of tested profiles L 150x150x18

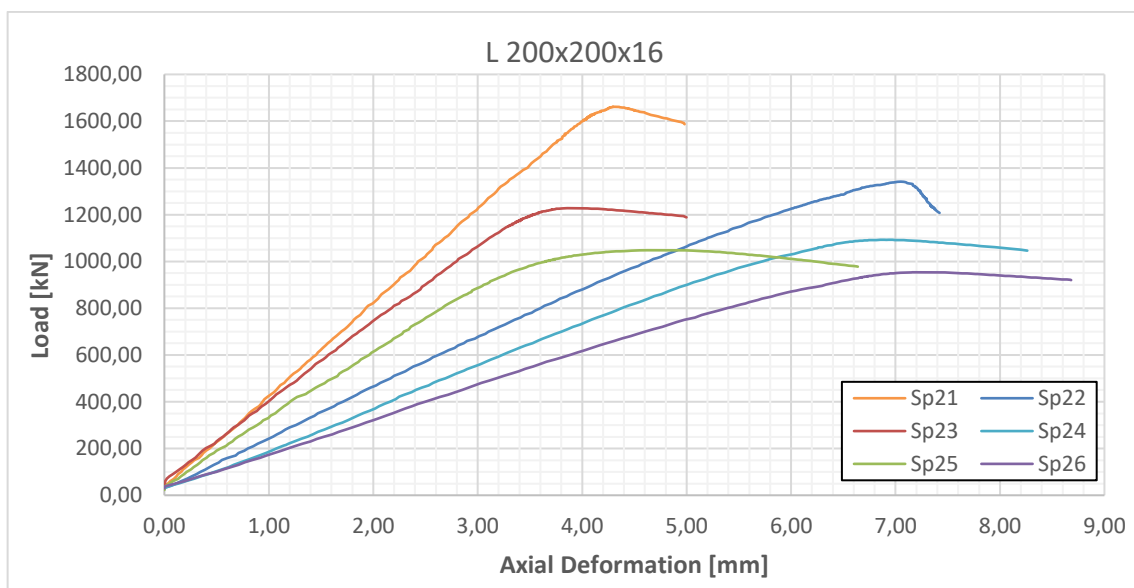


Figure 4.2: Load vs axial deformation of tested profiles L 200x200x16

## 4.2 Comparison with FEM results

A comparison of the stiffness and the ultimate resistance of the members obtained through the experiments and the numerical simulations, considering actual imperfections and geometrical/material properties, is presented below.

The numerical analyses of the test specimens have been performed with FINELG non-linear finite element software, using beam elements given the fact that no local buckling took place during the tests. The model and the boundary conditions are the same as for the preliminary studies. But to evaluate the actual critical length of the specimen, 107 mm (thicknesses of specimen's and machine's end plates) added to the length of all specimens. The FINELG finite element analyses adopting the GMNIA method were performed, considering:

- an initial member imperfection (shape and magnitude in accordance with the measured ones);
- the same pattern of residual stresses (see Figure 2.2);

- material laws in accordance with the measured ones (see Figure 3.9).

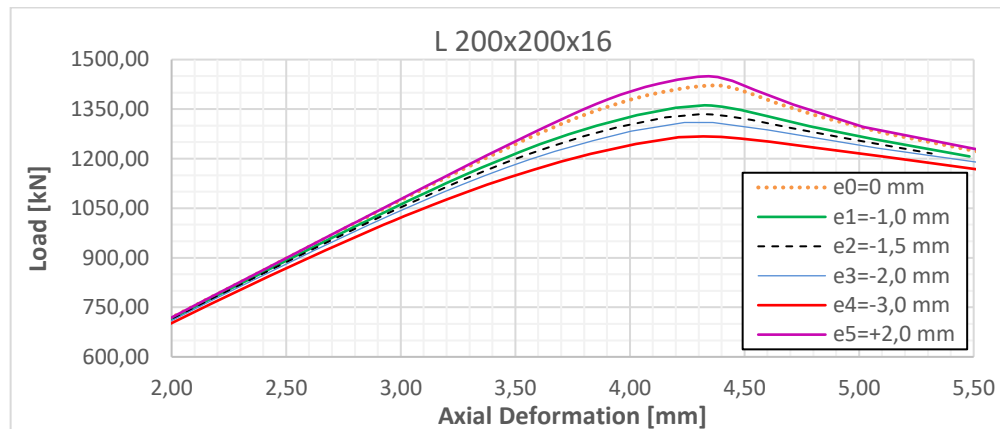


Figure 4.3: Influence of eccentricity at the ultimate resistance of member

A tolerance on the position of the applying load up to 2,0mm has been adopted for the numerical simulations. It has been found that even a small eccentricity could affect the ultimate resistance in comparison to the perfectly “no loading eccentricity” case. The influence of this small eccentricity of the applying load on the stiffness and the ultimate resistance has been also observed in [13]. Figure 4.3 shows that an eccentricity equals to 1,5mm is able to change the ultimate resistance by close to 6%. This tolerance could be explained by the two following reasons:

- the position of the load has been designed to be at the centre of the end plates and in such a way that the point coincides with the centre of gravity of the cross section. But in reality, due to small differences of the cross-section geometry, the real centre of gravity does not coincide exactly with the point of loading.
- the positioning of the specimen in the testing rig may also induce a small and unexpected eccentricity.

Figure 4.4 and Figure 4.5 compare the experimental response of each specimen with the numerical one obtained through FEM, and the results are reported also in Table 4.1.

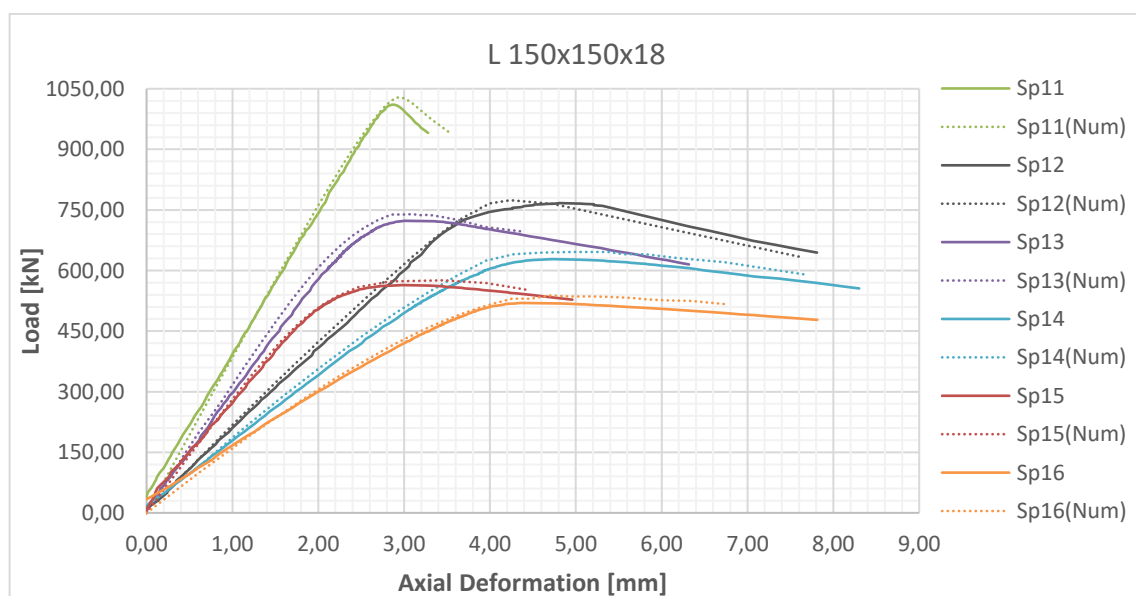


Figure 4.4: Comparison between test and FEM results for Sp1#

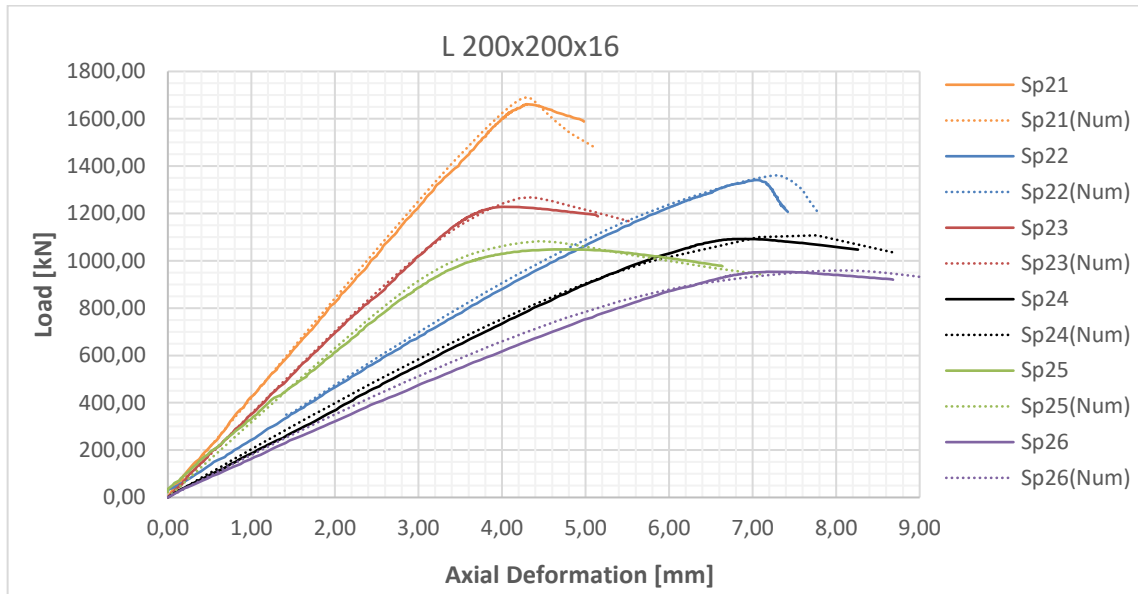


Figure 4.5: Comparison between test and FEM results for Sp2#

Table 4.1: Comparison between ultimate resistances obtained through tests and finite element models

ID of Specimen	Profile	P <sub>exp</sub> [kN]	P <sub>FEM</sub> [kN]	P <sub>exp</sub> /P <sub>FEM</sub>
Sp11	150x150x18	1010,57	1028,551	0,98
Sp12	150x150x18	767,34	774,069	0,99
Sp13	150x150x18	723,19	739,334	0,98
Sp14	150x150x18	628,27	645,853	0,97
Sp15	150x150x18	563,91	575,848	0,98
Sp16	150x150x18	519,76	535,994	0,97
Sp21	200x200x16	1661,54	1690,556	0,98
Sp22	200x200x16	1341,35	1360,96	0,99
Sp23	200x200x16	1227,96	1267,427	0,97
Sp24	200x200x16	1092,28	1107,591	0,99
Sp25	200x200x16	1048,07	1082,229	0,97
Sp26	200x200x16	953,62	959,145	0,99

It is obvious from Figure 4.4, Figure 4.5 as well as Table 4.1 that there is a very good agreement between the numerical simulations and the experimental results in terms of stiffness and ultimate resistances (less than 3%).

### 4.3 Comparison with Eurocode 3

As already mentioned in §2.1, the first profile (L 150x150x18) is classified as Class 1 and the second one (L 200x200x16) as Class 4, even if no plate buckling has been reported during the tests.

Figure 4.6 presents the experimental results (only for centrally loaded specimens) compared with those obtained through the present recommendations of EN1993-1-1; reference buckling curves a<sub>0</sub>, a and b are reported too.

The buckling reduction factor  $\chi$  of specimens has been calculated by the equation:

$$\chi = \frac{P_{ult}}{P_{pl}} = \frac{P_{ult}}{A \cdot f_y} \quad (\text{eq.18})$$

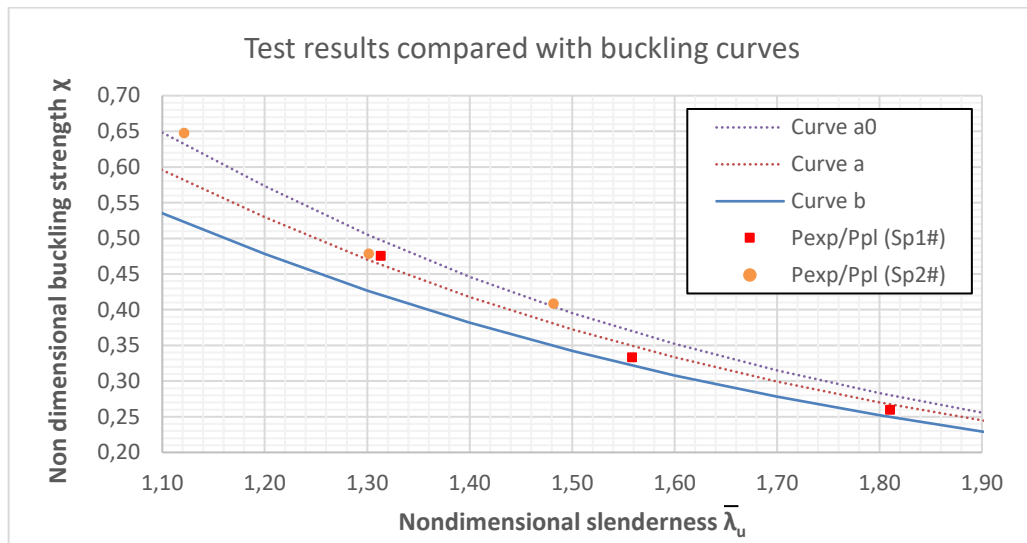


Figure 4.6: Comparison of experimental results with buckling curves of EN1993-1-1

and the reduced (non-dimensional) slenderness  $\bar{\lambda}_u$  has been obtained by:

$$\bar{\lambda}_u = \sqrt{\frac{N_{pl}}{N_{cr}}} \quad (\text{eq.19})$$

where  $N_{cr}$  is the elastic critical load for the relevant buckling mode (i.e. the minimum eigenvalue amongst all flexural and flexural-torsional buckling modes), obtained through an elastic instability analysis considering actual material and gross cross-section properties. A pure torsional mode cannot be obtained for a centrally loaded angle column as explained in [14]. The actual yielding stress  $f_y$  has been used for the non-linear calculations. Table 4.2 includes the results from the calculations indicated in Figure 4.6.

Table 4.2: Nondimensional slenderness  $\lambda$  and reduction factor  $\chi$  calculations

ID of Specimen	A [mm <sup>2</sup> ]	N <sub>cr</sub> [kN]	$\bar{\lambda}_u$ [-]	$\chi$ [-]	P <sub>exp</sub> [kN]	P <sub>pl</sub> [kN]	P <sub>EC3</sub> [kN]	P <sub>exp</sub> /P <sub>EC3</sub>	P <sub>exp</sub> /P <sub>pl</sub>
Sp11	5100,0	1233,7	1,313	0,4206	1010,57	2128	894,8	1,13	0,4749
Sp13	5101,2	894,302	1,558	0,3216	723,19	2172	698,5	1,04	0,3329
Sp15	5106,5	663,551	1,810	0,2496	563,91	2174	542,7	1,04	0,2593
Sp21	6180,2	2040,9	1,122	0,5224	1661,54	2567	1341,3	1,24	0,6472
Sp23	6181,3	1515,1	1,302	0,4260	1227,96	2568	1093,8	1,12	0,4782
Sp25	6180,1	1168,6	1,482	0,3489	1048,07	2567	895,6	1,17	0,4082

According to Eurocode 3, the buckling curve b has been selected for axially loaded equal angle columns (solid line in Figure 4.6). It has been found that the experimental results are in line with this curve or above. Furthermore, it can be easily observed that the actual ultimate resistance of all centrally load columns is equal or higher than the predictions of Eurocode; the latter seems so to provide safe evaluations (see Table 4.2), especially for specimens Sp2# where the detrimental effects of local buckling are possibly overestimated.

## 5 Conclusions

From this experimental program and the accompanying numerical/analytical studies, following conclusions may be drawn:

- Flexural buckling governs and leads the specimens into failure. For specimens without loading eccentricity a pure flexural buckling has occurred while specimens with load eccentricity reached failure in a flexural-torsional buckling mode. In fact, the column cross-section twists at the beginning of loading, and then laterally deforms according to a flexural buckling at later loading stages, until failure.
- Local buckling was not observed at any specimen, although one of them was categorized as class 4 according to EN1993-1-1.
- A very good agreement between numerical GMNIA simulations and experimental results in terms of stiffness and ultimate resistances has been achieved.
- A small eccentricity of the position of the applying load can affect the ultimate resistance of the member in comparison with the perfect “no loading eccentricity” case. For the current study, an eccentricity equal to 1,5 mm may reduce the ultimate resistance by about 6%.
- The design resistance of the specimens based on EN1993-1-1 and EN1993-1-5 is on the safe side, especially for the second profile for which the local buckling reduction effects seem to be overestimated by Eurocode.

## **References**

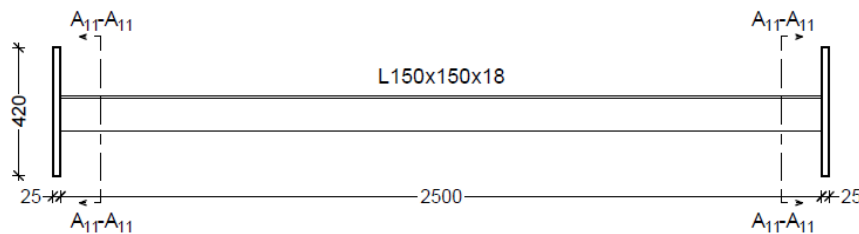
- [1] Spiliopoulos A, Dasiou M-E, Thanopoulos P, Vayas I, Experimental tests on members made from rolled angle sections, *Steel Construction – Design and Research*, Vol.11, Issue 1, pp. 84-93, 2018.
- [2] Ban H.Y, Shi G, Shi Y.J, Wang Y.Q, Column buckling tests of 420MPa high strength steel single equal angles. *International Journal of Structural Stability and Dynamics*, Vol.13, 2013.
- [3] EN1993-1-1 (2005). *Design of steel structures. Part 1-1 General rules and rules for buildings*, Brussels, Comité Européen de Normalisation (CEN).
- [4] EN1993-1-5: *Design of steel structures - Part 1-5: Plate structural elements*, Brussels, Comité Européen de Normalisation (CEN), 2006.
- [5] Zhang L, Jaspart JP, *Stability of members in compression made of large hot-rolled and welded angles*, Université de Liège, 2013.
- [6] FINELG: *Non-linear finite element analysis program, User's manual, Version 9.0*, Greisch Ingenieure, 2003.
- [7] EN1993-1-8: *Design of steel structures - Part 1-8: Design of joints*. Brussels. Comité Européen de Normalisation (CEN), 2005.
- [8] ISO 1090-2: *Technical requirements for the execution of steel structures*, Comité Européen de Normalisation (CEN), 2008
- [9] prEN1993-1-14 (20XX): XXXX, Brussels. Comité Européen de Normalisation (CEN).
- [10] EN 10056-2 (1993). *Structural steel equal and unequal leg angles - Part 2: Tolerances on shape and dimensions*. Brussels. Comité Européen de Normalisation (CEN).
- [11] ISO 6892 – 1 (2016). *Metallic materials – Tensile testing – Part 1: Method of test at room temperature*, Brussels, Comité Européen de Normalisation (CEN).
- [12] EN ISO 377 (1997): *Steel and steel products — Location and preparation of samples and test pieces for mechanical testing*, Brussels, Comité Européen de Normalisation (CEN).
- [13] de Menezes AA, da S. Vellasco PCG, de Lima LRO, da Silva AT, *Experimental and numerical investigation of austenitic stainless steel hot-rolled angles under compression*, *Journal of Constructional Steel Research*, Vol.152, pp. 42-56, 2019.
- [14] de Ville de Goyet V, *L'analyse statique non linéaire par la méthode des éléments finis des structures spatiales formées de poutres à section non symétrique*, PhD thesis, University of Liège, 1989.

## Annex A

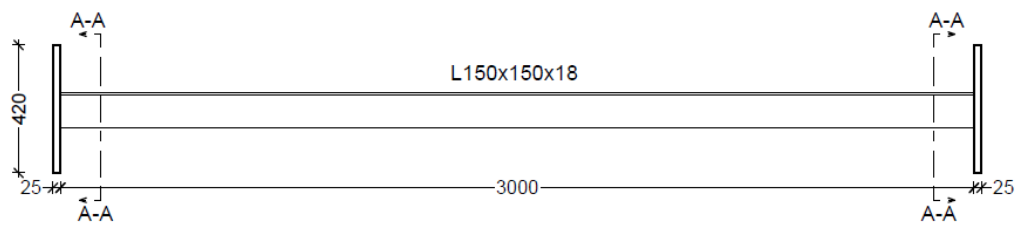
Annex A includes the drawing details of the specimens.

### A1. ANGLE COLUMNS PROFILE L150x150x18

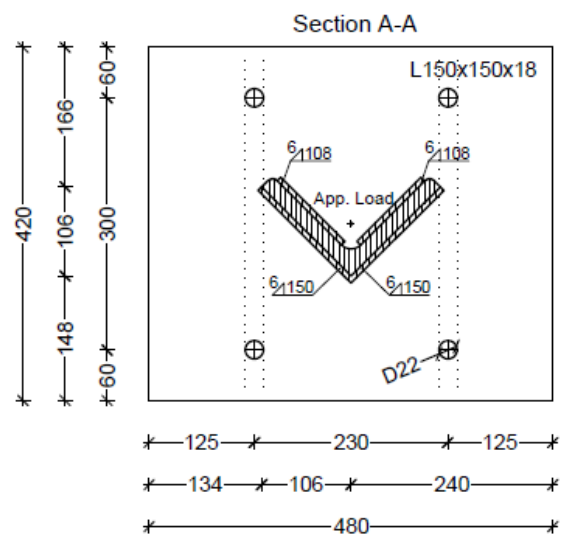
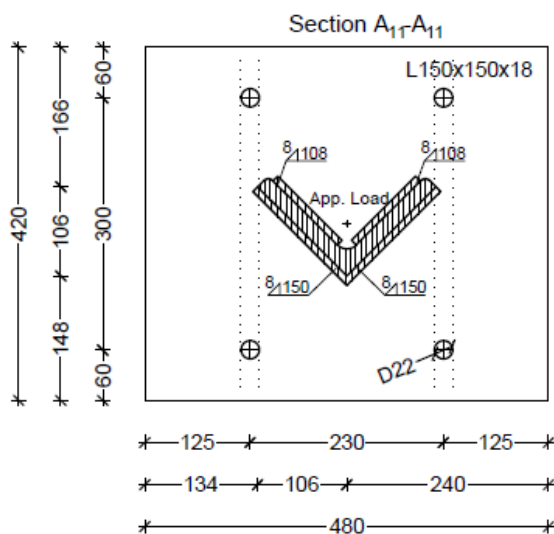
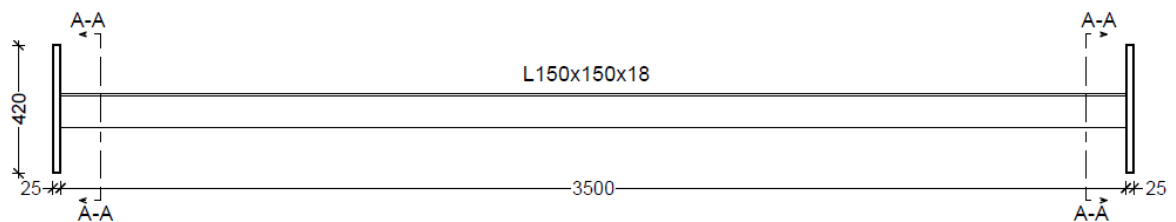
SPECIMEN 11



SPECIMEN 13

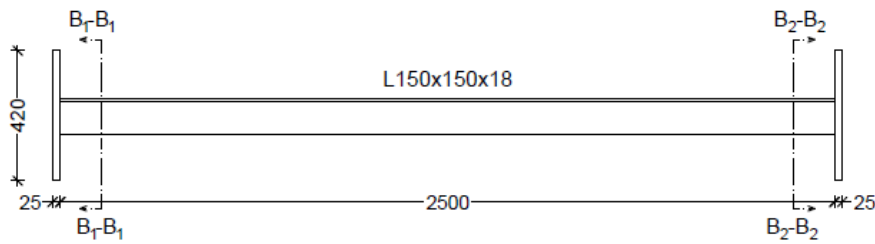


SPECIMEN 15

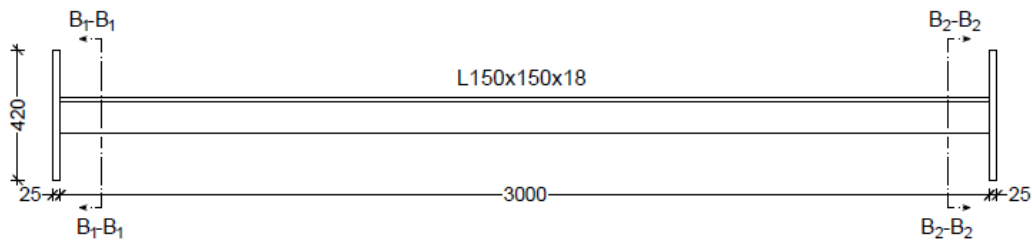




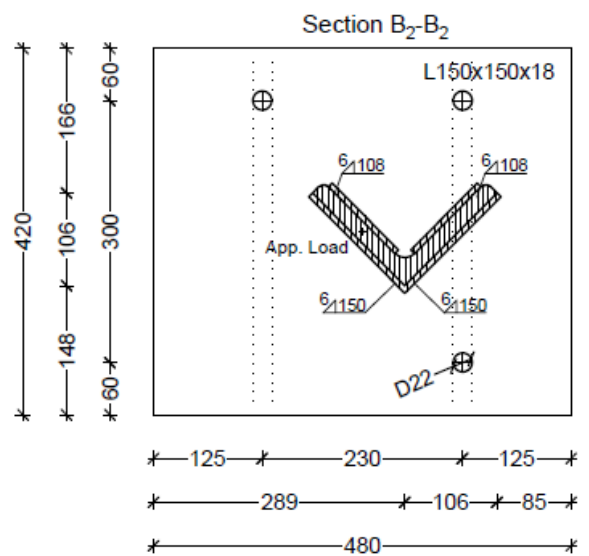
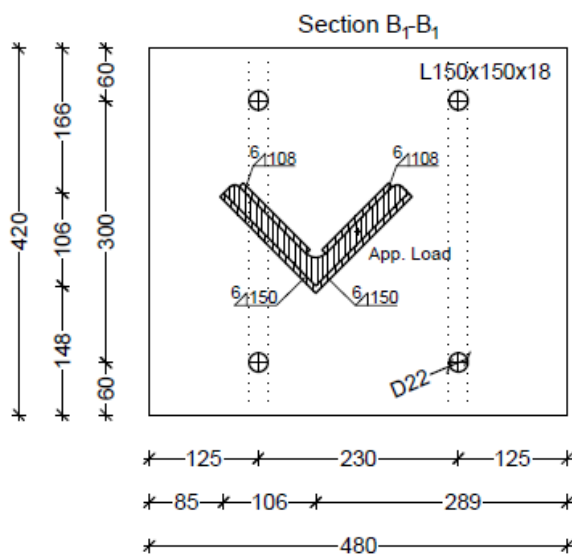
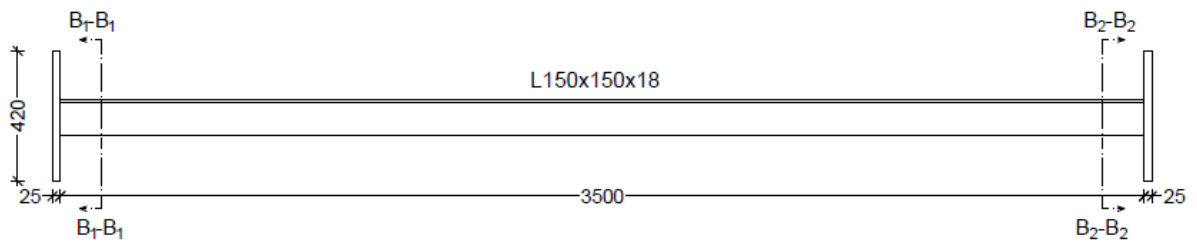
**SPECIMEN 12**



**SPECIMEN 14**

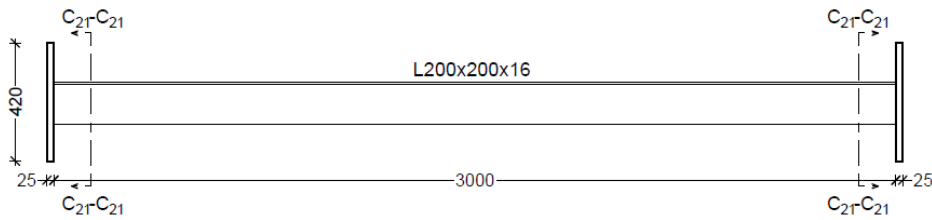


**SPECIMEN 16**

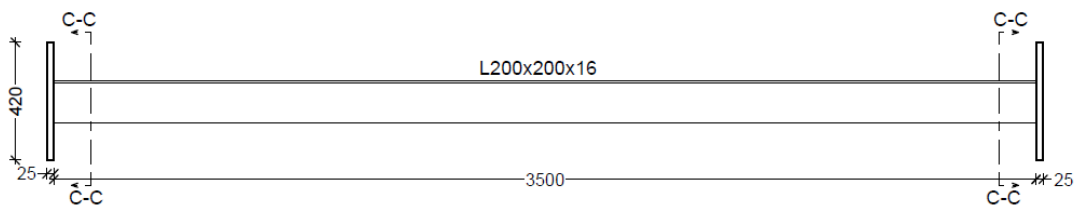


**A2. ANGLE COLUMNS PROFILE L200x200x16**

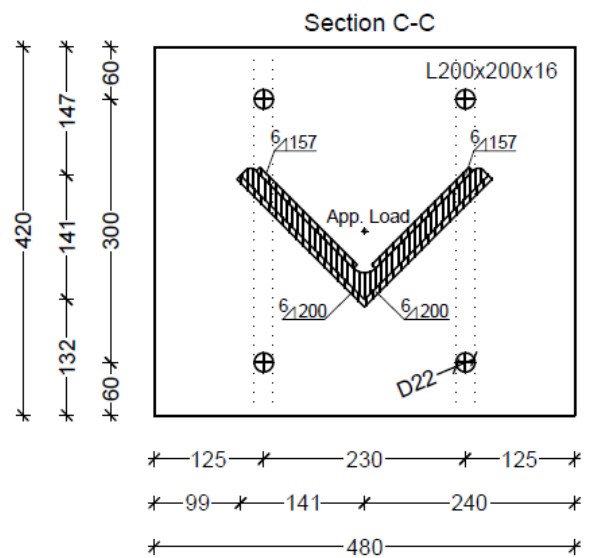
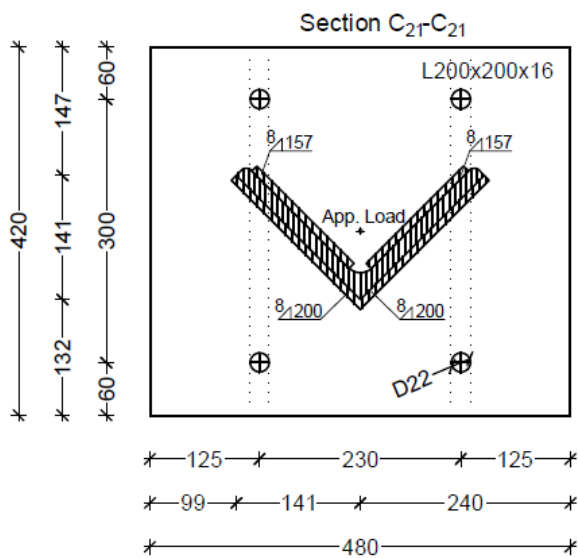
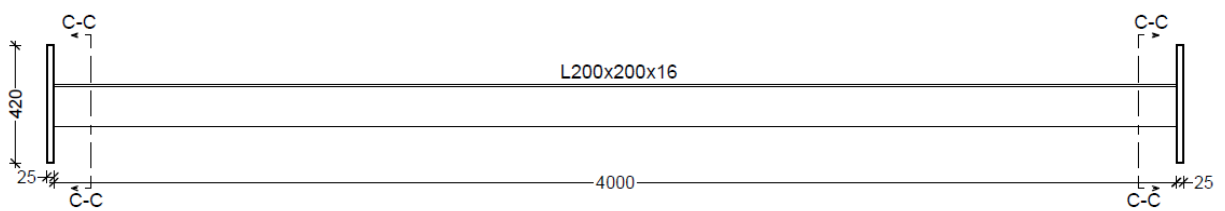
**SPECIMEN 21**



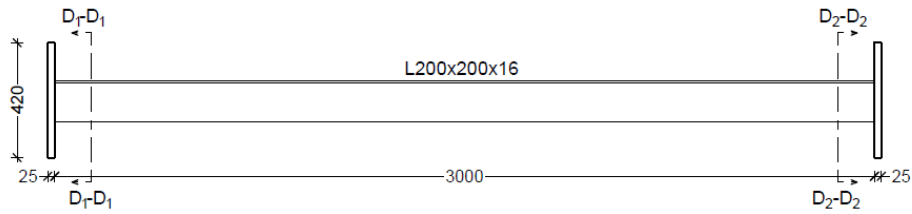
**SPECIMEN 23**



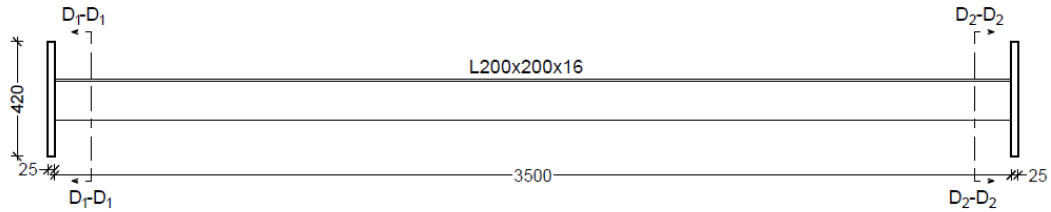
**SPECIMEN 25**



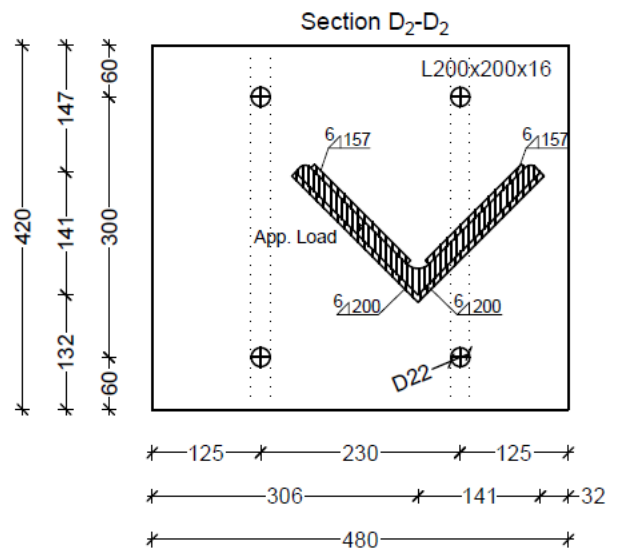
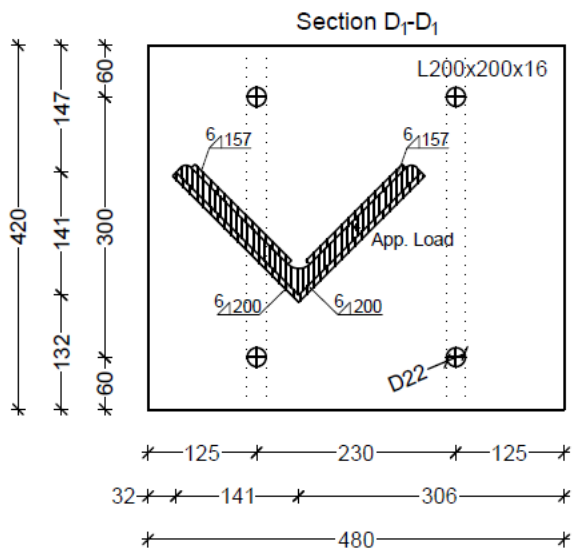
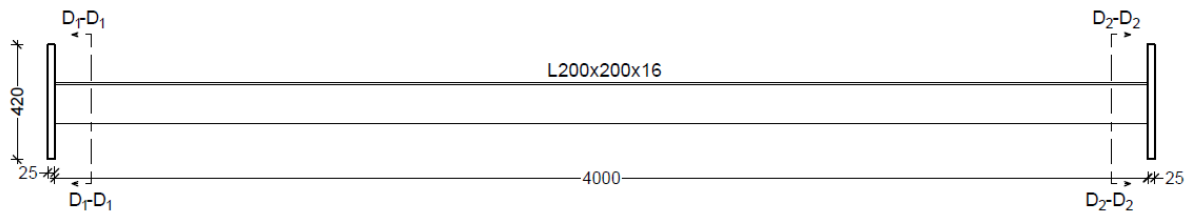
SPECIMEN 22



SPECIMEN 24



SPECIMEN 26



## Annex B

Annex B includes the details as well as the results (initial imperfections, load-displacements curves, strain gauges) of each specimen.


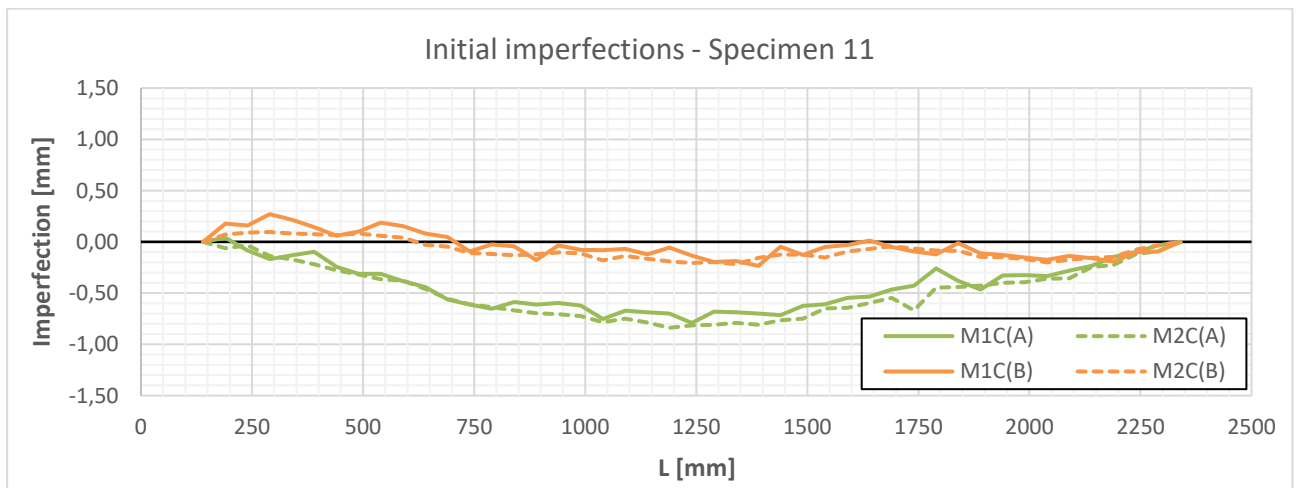
### **B0. Symbols and definitions**

The symbols that are used in graphs and tables of the current annex, are summarized below:

$t_1$	is the thickness of leg 1 (Face A) of the cross-section;
$t_2$	is the thickness of leg 2 (Face B) of the cross-section;
$b_1$	is the width of leg 1 (Face A) of the cross-section;
$b_2$	is the width of leg 1 (Face B) of the cross-section;
$L$	is the length of the specimen $i$ between the end plates;
$L_{crit}$	is the critical (buckling) length of the specimen $i$ between the joints;
$e_u$	is the eccentricity of the applying load along $u$ principal axis;
$e_v$	is the eccentricity of the applying load along $v$ principal axis;
$f_y$	is the actual yielding stress (limit of elasticity value);
$M1C(A)$	is the M1 corrected measurement on face A for specimen $i$ ;
$M2C(A)$	is the M2 corrected measurement on face A for specimen $i$ ;
$M1C(B)$	is the M1 corrected measurement on face B for specimen $i$ ;
$M2C(B)$	is the M2 corrected measurement on face B for specimen $i$ ;
$U_{O,midH}$	is the displacement of the corner point O of the mid – height cross-section along $u$ principal axis;
$V_{O,midH}$	is the displacement of the corner point O of the mid – height cross-section along $v$ principal axis;
$U_{O,lowH}$	is the displacement of the corner point O of the low – height cross-section along $u$ principal axis;
$V_{O,lowH}$	is the displacement of the corner point O of the low – height cross-section along $v$ principal axis;
$\theta_{mean,midH}$	is the mean torsional rotation $[(\theta_A+\theta_B)/2]$ at the mid – height cross-section;
$\theta_{mean,lowH}$	is the mean torsional rotation $[(\theta_A+\theta_B)/2]$ at the low – height cross-section;
$\Delta\phi_{midH}$	is the distortion $(\theta_B-\theta_A)$ at the mid – height cross-section;
$\Delta\phi_{lowH}$	is the distortion $(\theta_B-\theta_A)$ at the low – height cross-section;

**B1. Specimen Sp11**

ID of specimen: Sp11	
Date of testing	25/10/2019
Type of test	Centrally loaded compression test
Mean actual dimensions	
Cross-section	L150x150x18
t <sub>1</sub> [mm]	18,04
t <sub>2</sub> [mm]	18,17
b <sub>1</sub> [mm]	150,09
b <sub>2</sub> [mm]	150,10
L [mm]	2500,00
L <sub>crit</sub> [mm]	2500+107=2607,00
Eccentricity e <sub>u</sub> [mm]	0,00
Eccentricity e <sub>v</sub> [mm]	0,00
Material	
Material	S 460/3
Actual f <sub>y</sub> [Mpa]	417,2
Actual f <sub>u</sub> [Mpa]	560,9
Response	
Ultimate resistance [kN]	1010,57
Failure mode / Comments	Flexural Buckling

**Figure B.1: Initial imperfections of both faces along specimen 11**

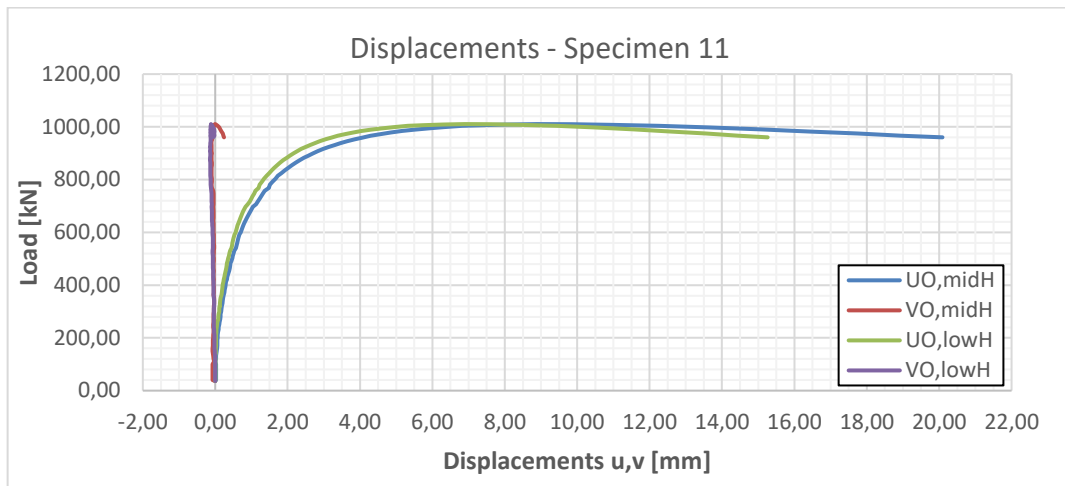


Figure B.2: Displacements of the corner point O along the principal axis, at mid-height and lower height (1/4H) cross-sections, for specimen 11

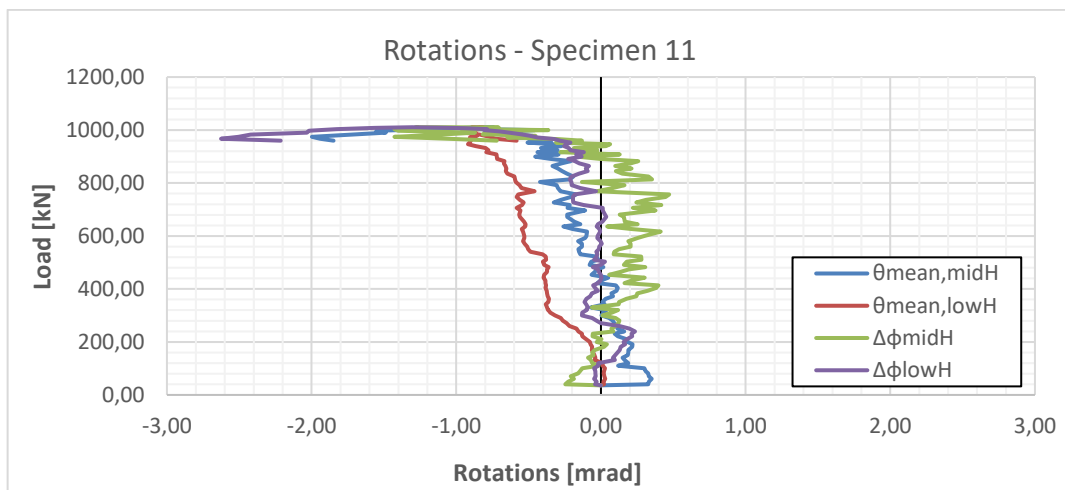


Figure B.3: Rotation along the length axe of two cross-sections along specimen 11

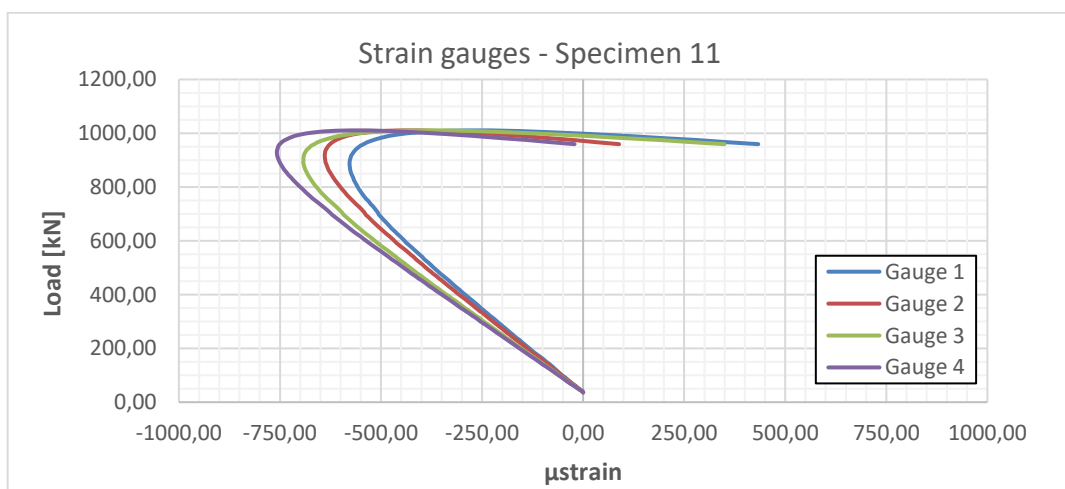

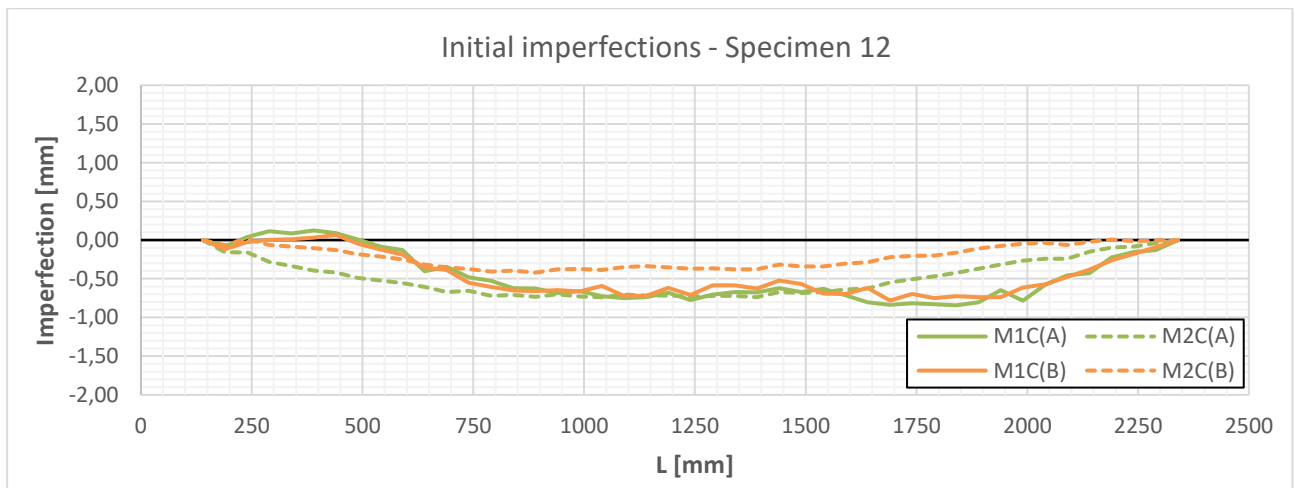


Figure B.4: Measurements of strain gauges on specimen 11

**B2. Specimen Sp12**

ID of specimen: Sp12	
Date of testing	13/05/2019
Type of test	Eccentrically loaded compression test
Mean actual dimensions	
Cross-section	L150x150x18
t <sub>1</sub> [mm]	18,18
t <sub>2</sub> [mm]	18,04
b <sub>1</sub> [mm]	150,07
b <sub>2</sub> [mm]	150,12
L [mm]	2500,00
L <sub>crit</sub> [mm]	2500+107=2607,00
Eccentricity e <sub>u</sub> [mm]	0,00
Eccentricity e <sub>v</sub> [mm]	48,74
Material	
Material	S 460/1
Actual f <sub>y</sub> [Mpa]	425,8
Actual f <sub>u</sub> [Mpa]	572,5
Response	
Ultimate resistance [kN]	767,34
Failure mode / Comments	Flexural-Torsional Buckling

**Figure B.5: Initial imperfections of both faces along specimen 12**



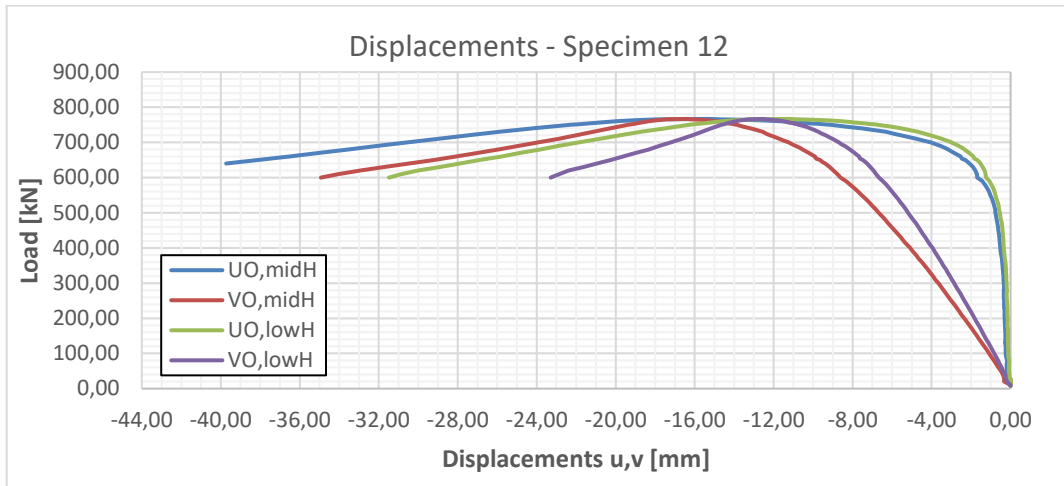


Figure B.6: Displacements of the corner point O along the principal axis, at mid-height and lower height (1/4H) cross-sections, for specimen 12

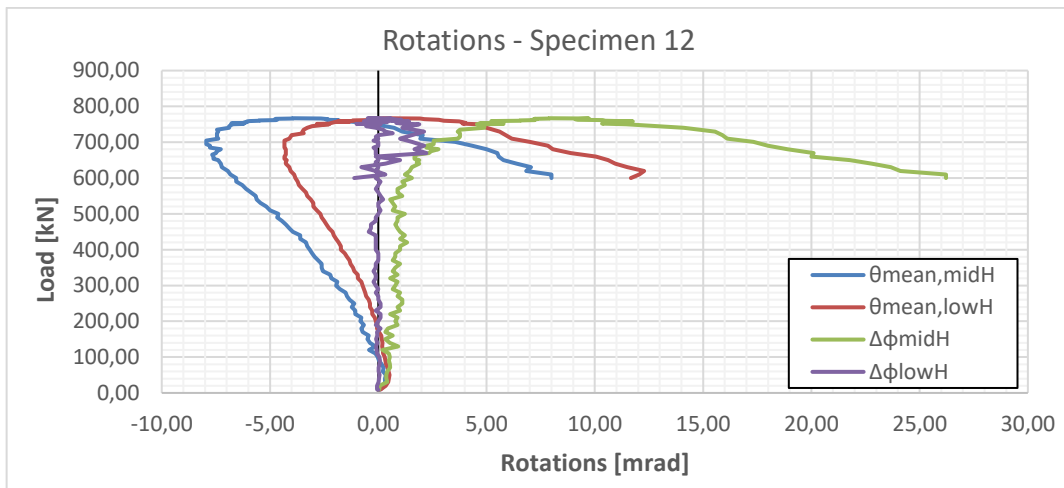


Figure B.7: Rotation along the length axe of two cross-sections along specimen 12

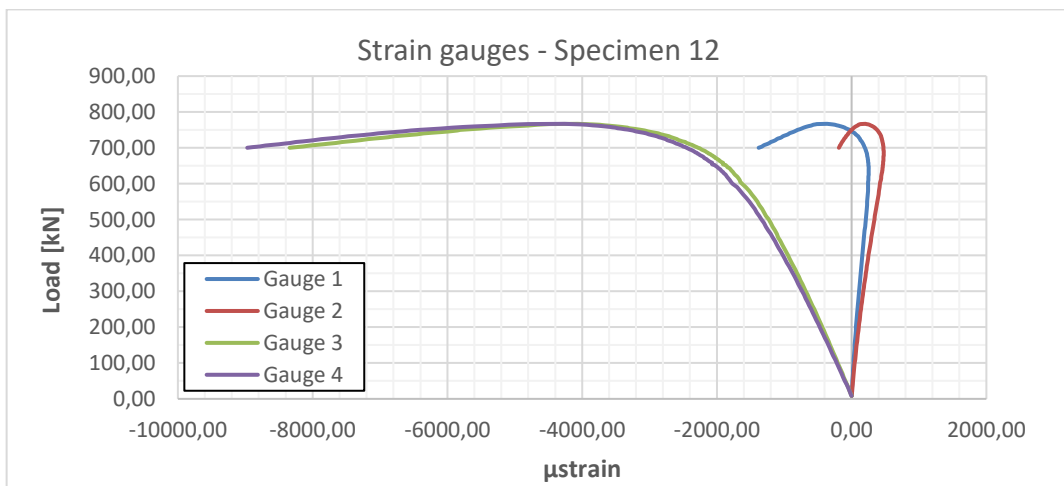

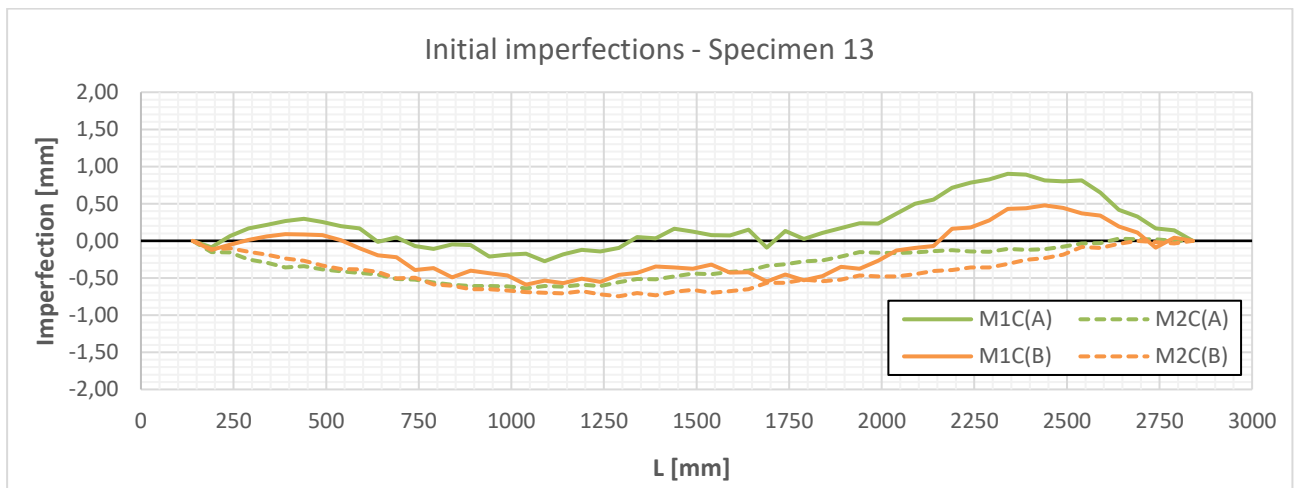


Figure B.8: Measurements of strain gauges on specimen 12



**B3. Specimen Sp13**

ID of specimen: Sp13	
Date of testing	14/05/2019
Type of test	Centrally loaded compression test
Mean actual dimensions	
Cross-section	L150x150x18
t <sub>1</sub> [mm]	18,04
t <sub>2</sub> [mm]	18,16
b <sub>1</sub> [mm]	150,11
b <sub>2</sub> [mm]	149,92
L [mm]	3000,00
L <sub>crit</sub> [mm]	3000+107=3107,00
Eccentricity e <sub>u</sub> [mm]	0,00
Eccentricity e <sub>v</sub> [mm]	0,00
Material	
Actual f <sub>y</sub> [Mpa]	425,8
Actual f <sub>u</sub> [Mpa]	572,5
Response	
Ultimate resistance [kN]	723,19
Failure mode / Comments	Flexural Buckling

**Figure B.9: Initial imperfections of both faces along specimen 13**

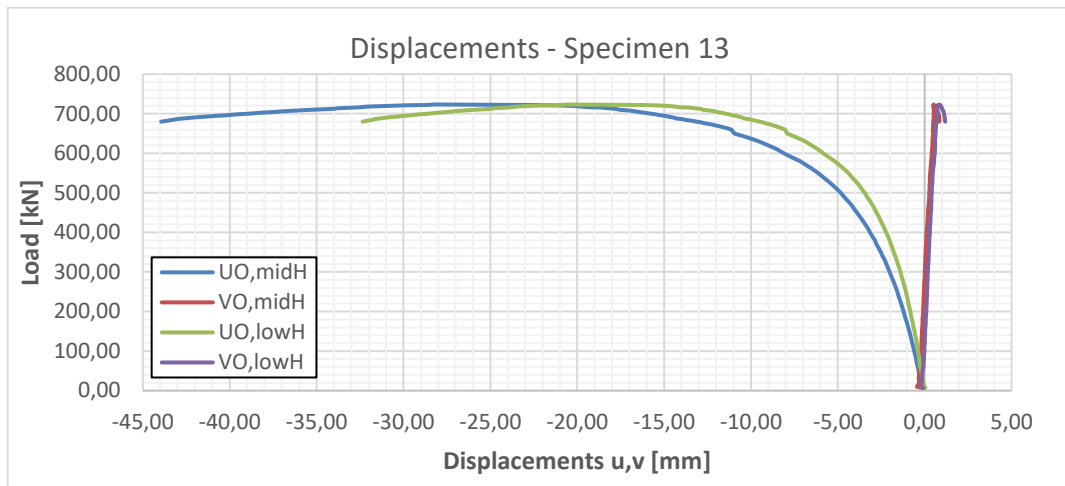


Figure B.10: Displacements of the corner point O along the principal axis, at mid-height and lower height (1/4H) cross-sections, for specimen 13

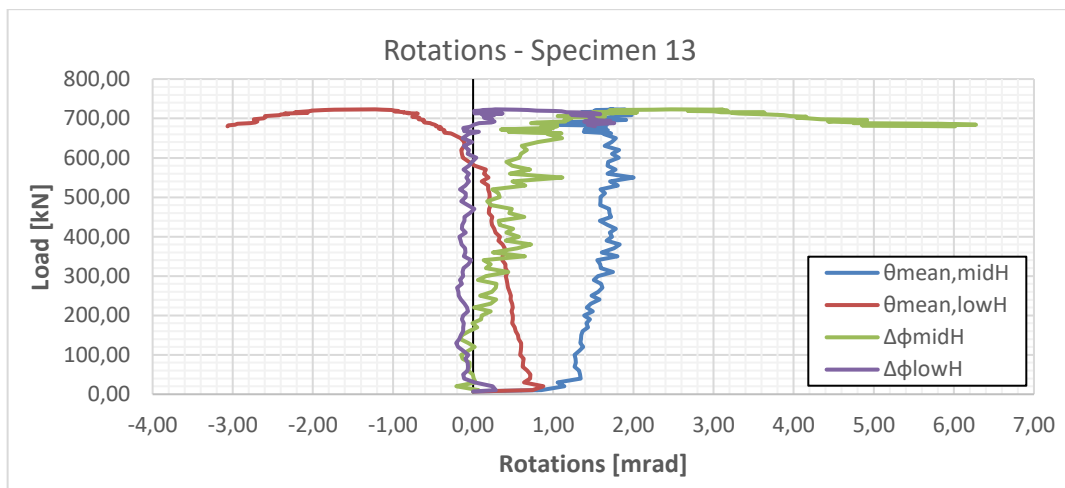


Figure B.11: Rotation along the length axe of two cross-sections along specimen 13

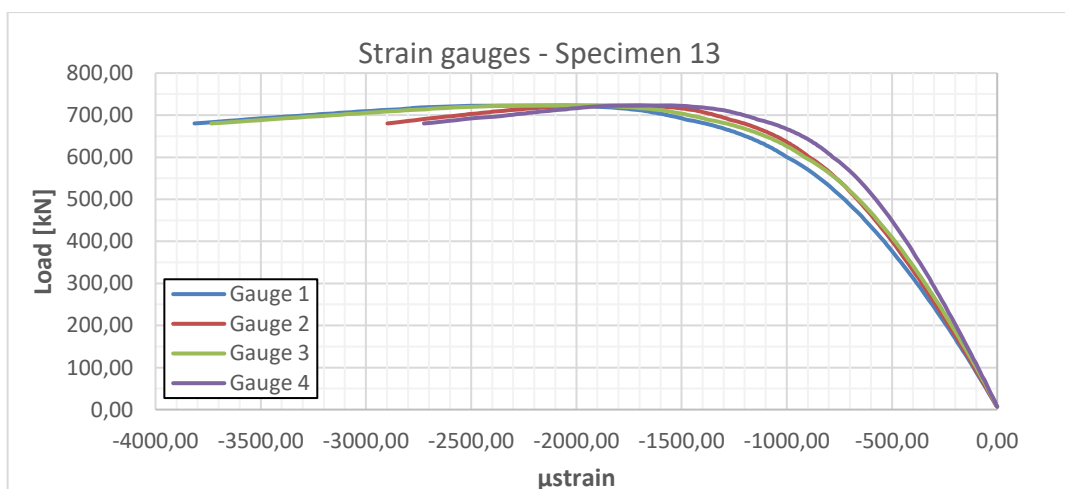
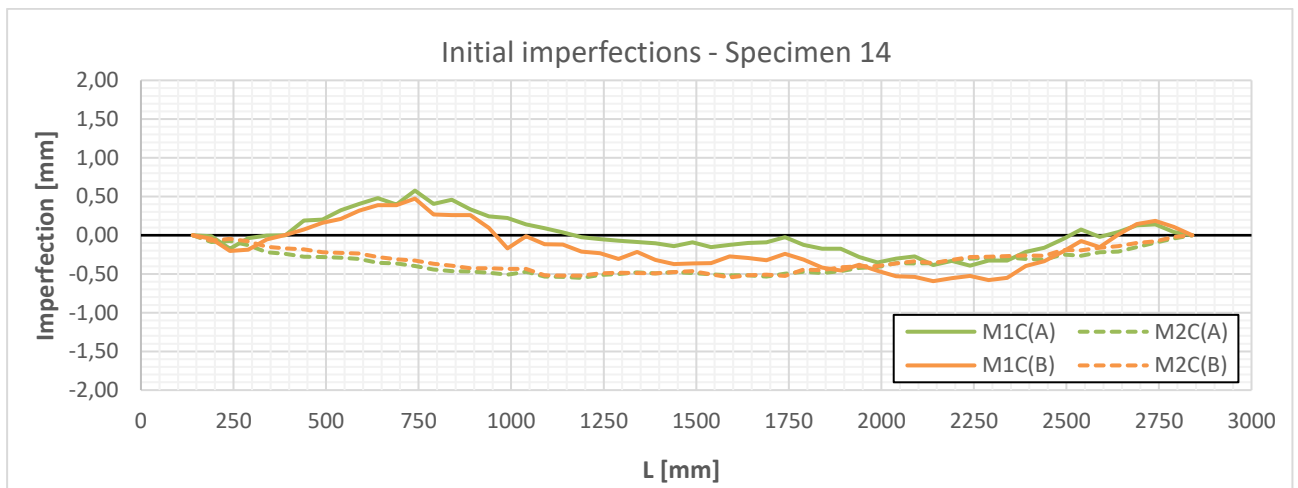


Figure B.12: Measurements of strain gauges on specimen 13

**B4. Specimen Sp14**

ID of specimen: Sp14	
Date of testing	15/05/2019
Type of test	Eccentrically loaded compression test
Mean actual dimensions	
Cross-section	L150x150x18
$t_1$ [mm]	18,04
$t_2$ [mm]	18,17
$b_1$ [mm]	150,09
$b_2$ [mm]	150,10
L [mm]	3000,00
$L_{crit}$ [mm]	$3000+107=3107,00$
Eccentricity $e_u$ [mm]	0,00
Eccentricity $e_v$ [mm]	48,74
Material	
Material	S 460/1
Actual $f_y$ [Mpa]	425,8
Actual $f_u$ [Mpa]	572,5
Response	
Ultimate resistance [kN]	628,27
Failure mode / Comments	Flexural-Torsional Buckling



**Figure B.13: Initial imperfections of both faces along specimen 14**

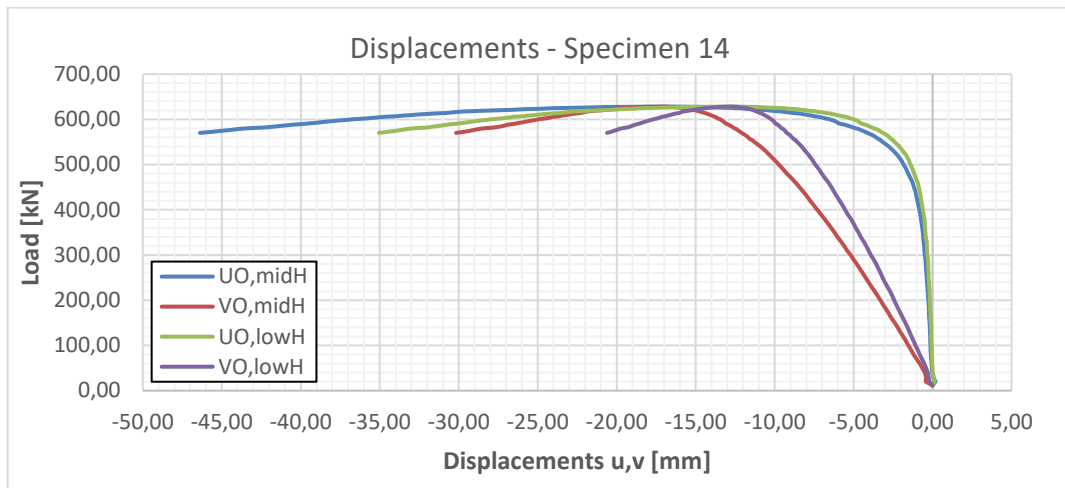


Figure B.14: Displacements of the corner point O along the principal axis, at mid-height and lower height (1/4H) cross-sections, for specimen 14

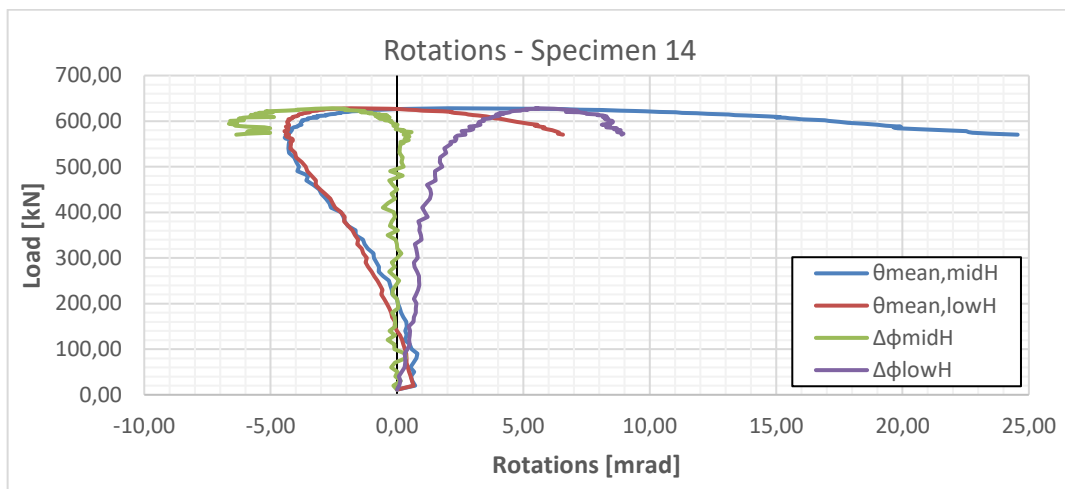


Figure B.15: Rotation along the length axe of two cross-sections along specimen 14

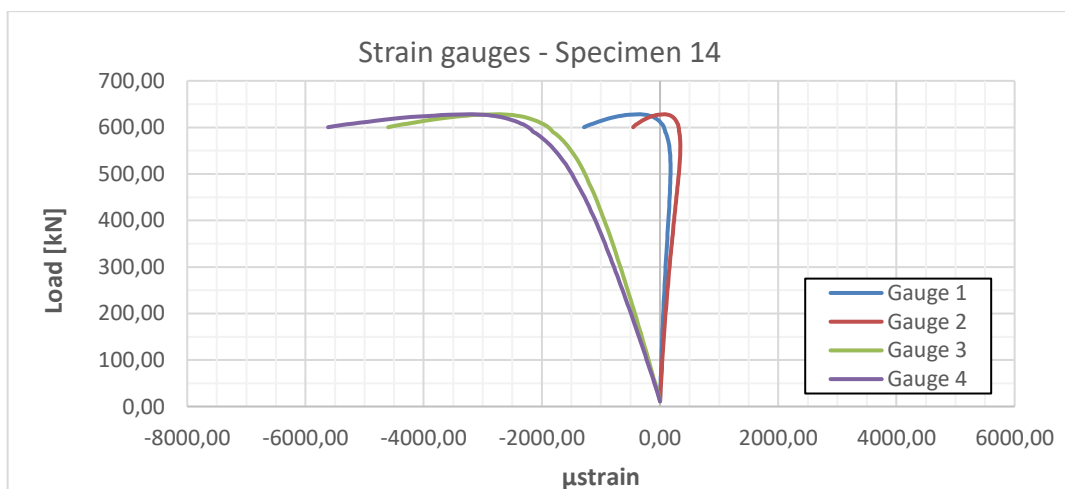



Figure B.16: Measurements of strain gauges on specimen 14

**B5. Specimen Sp15**

ID of specimen: Sp15	
Date of testing	16/05/2019
Type of test	Centrally loaded compression test
Mean actual dimensions	
Cross-section	L150x150x18
t <sub>1</sub> [mm]	18,17
t <sub>2</sub> [mm]	18,07
b <sub>1</sub> [mm]	150,07
b <sub>2</sub> [mm]	150,11
L [mm]	3500,00
L <sub>crit</sub> [mm]	3500+107=3607,00
Eccentricity e <sub>u</sub> [mm]	0,00
Eccentricity e <sub>v</sub> [mm]	0,00
Material	
Actual f <sub>y</sub> [Mpa]	425,8
Actual f <sub>u</sub> [Mpa]	572,5
Response	
Ultimate resistance [kN]	563,91
Failure mode / Comments	Flexural Buckling




**Figure B.17: Initial imperfections of both faces along specimen 15**

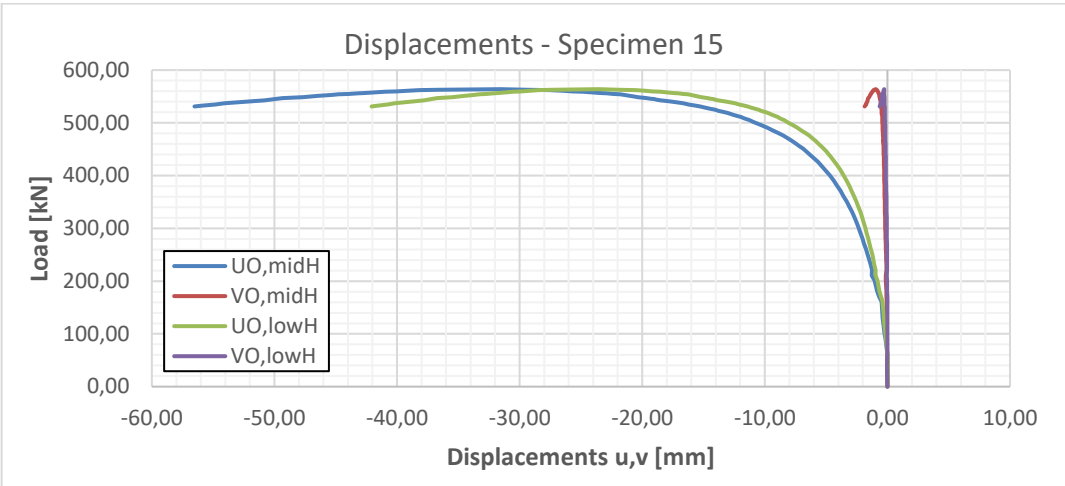


Figure B.18: Displacements of the corner point O along the principal axis, at mid-height and lower height (1/4H) cross-sections, for specimen 15

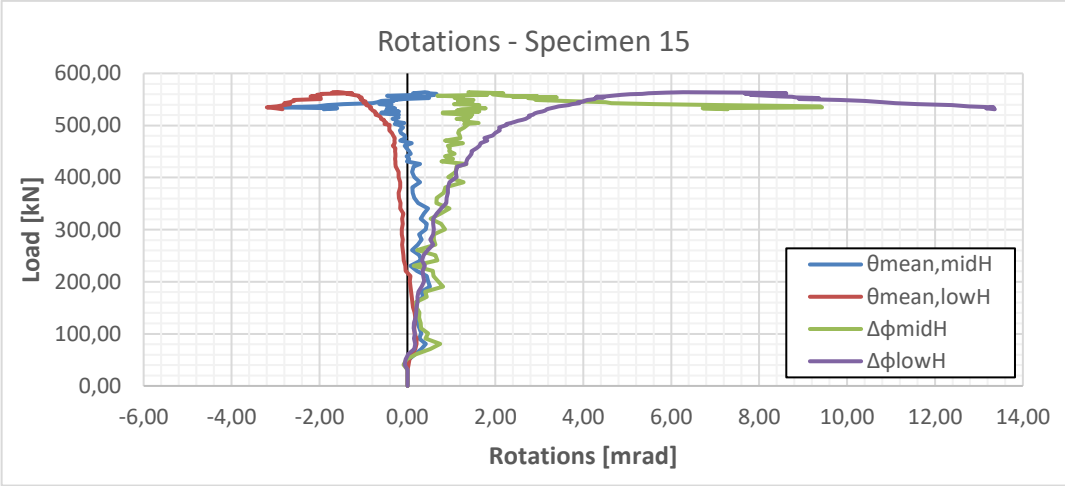


Figure B.19: Rotation along the length axe of two cross-sections along specimen 15

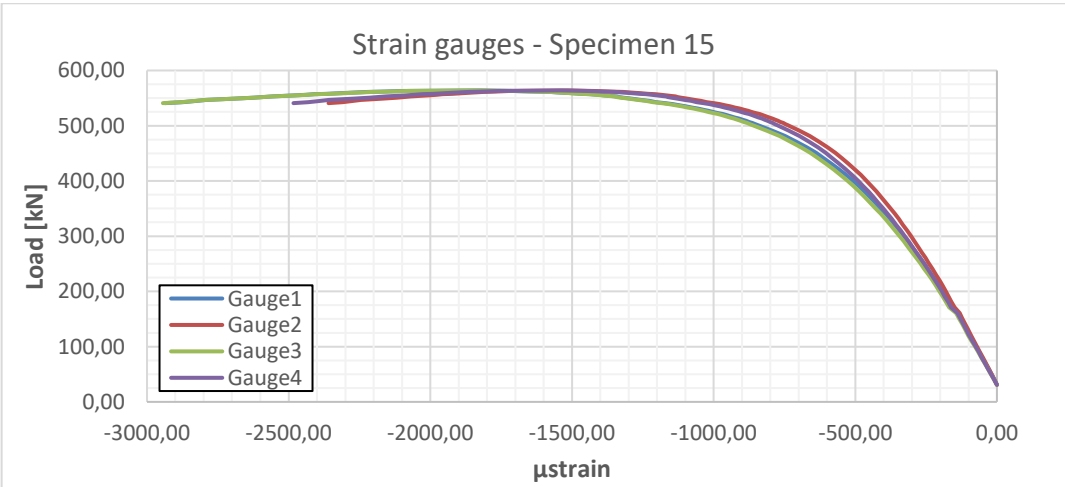
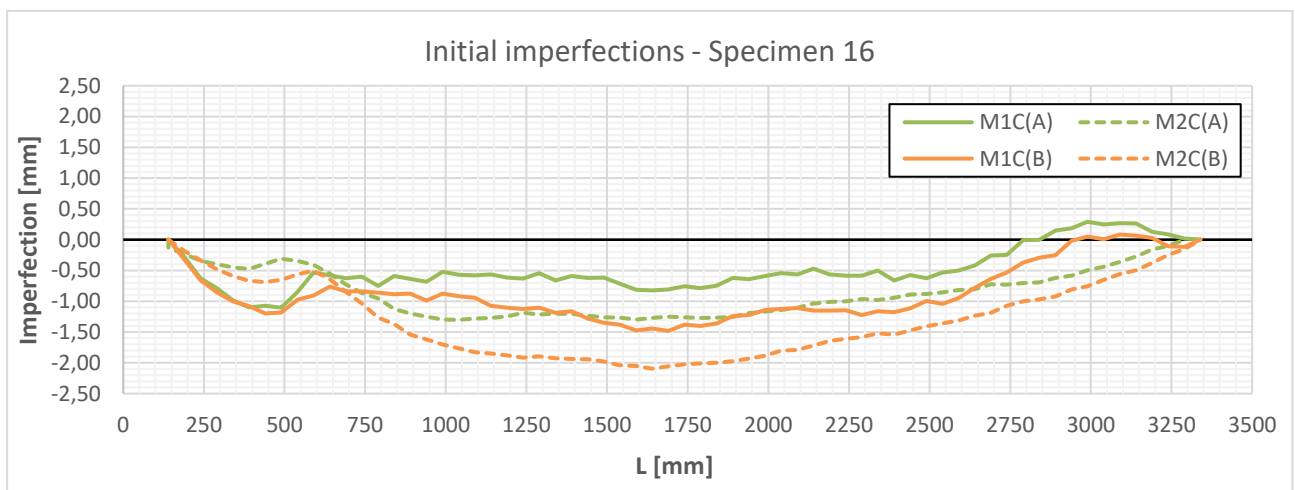


Figure B.20: Measurements of strain gauges on specimen 15



**B6. Specimen Sp16**

ID of specimen: Sp16	
Date of testing	16/05/2019
Type of test	Eccentrically loaded compression test
Mean actual dimensions	
Cross-section	L150x150x18
$t_1$ [mm]	18,16
$t_2$ [mm]	18,19
$b_1$ [mm]	150,11
$b_2$ [mm]	149,95
L [mm]	3500,00
$L_{crit}$ [mm]	$3500+107=3607,00$
Eccentricity $e_u$ [mm]	0,00
Eccentricity $e_v$ [mm]	48,74
Material	
Actual $f_y$ [Mpa]	425,8
Actual $f_u$ [Mpa]	572,5
Response	
Ultimate resistance [kN]	519,76
Failure mode / Comments	Flexural-Torsional Buckling



**Figure B.21: Initial imperfections of both faces along specimen 16**

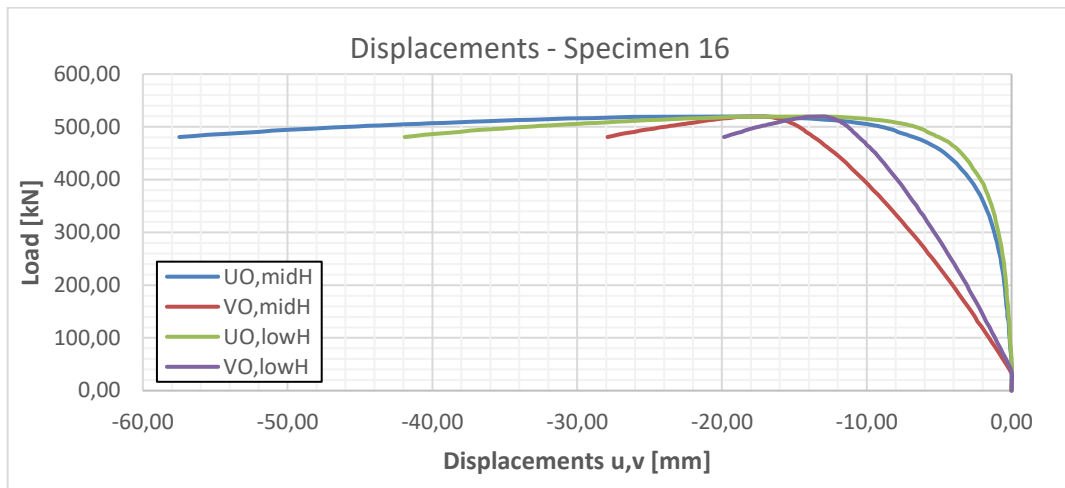


Figure B.22: Displacements of the corner point O along the principal axis, at mid-height and lower height (1/4H) cross-sections, for specimen 16

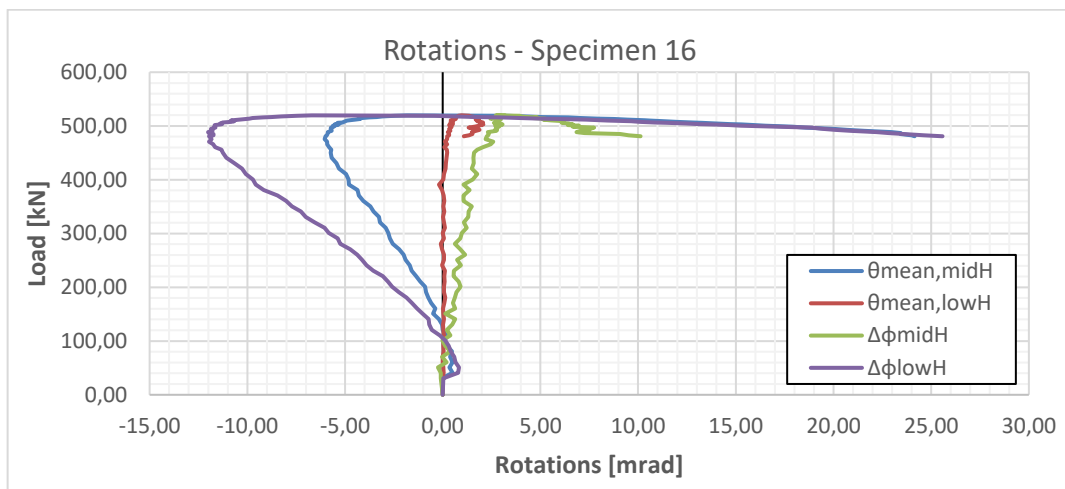


Figure B.23: Rotation along the length axe of two cross-sections along specimen 16

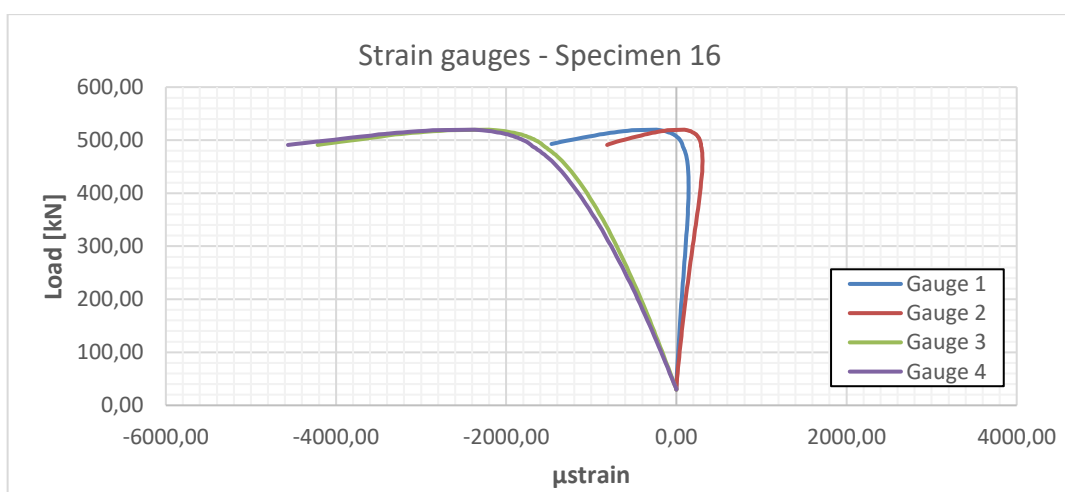

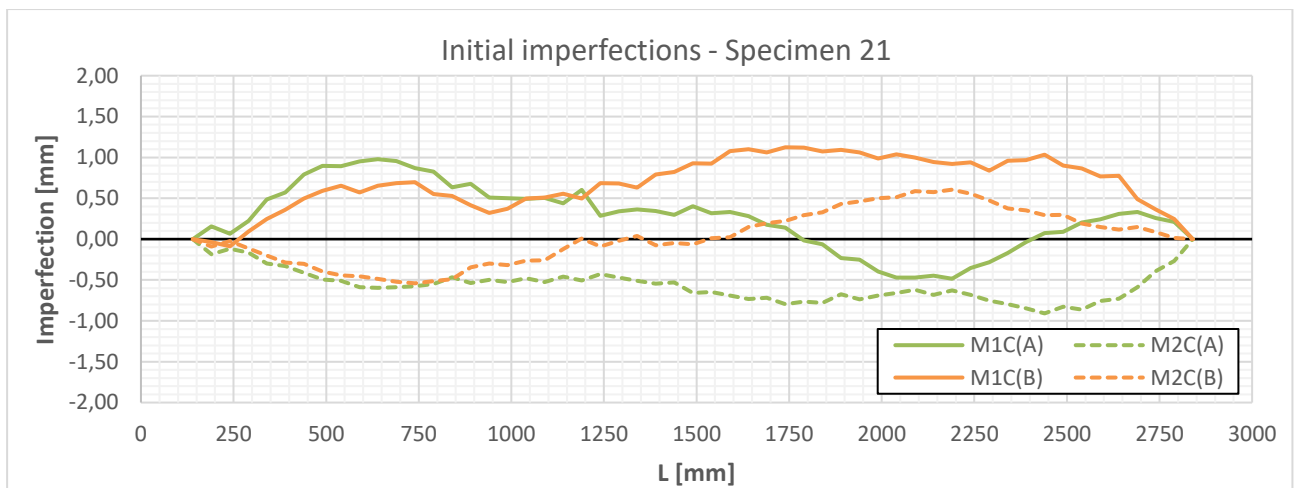


Figure B.24: Measurements of strain gauges on specimen 16



**B7. Specimen Sp21**

ID of specimen: Sp21	
Date of testing	20/05/2019
Type of test	Centrally loaded compression test
Mean actual dimensions	
Cross-section	L200x200x16
t <sub>1</sub> [mm]	16,32
t <sub>2</sub> [mm]	16,34
b <sub>1</sub> [mm]	200,31
b <sub>2</sub> [mm]	200,41
L [mm]	3000,00
L <sub>crit</sub> [mm]	3000+107=3107,00
Eccentricity e <sub>u</sub> [mm]	0,00
Eccentricity e <sub>v</sub> [mm]	0,00
Material	
Actual f <sub>y</sub> [Mpa]	487,6
Actual f <sub>u</sub> [Mpa]	604,6
Response	
Ultimate resistance [kN]	1661,54
Failure mode / Comments	Flexural Buckling

**Figure B.25: Initial imperfections of both faces along specimen 21**

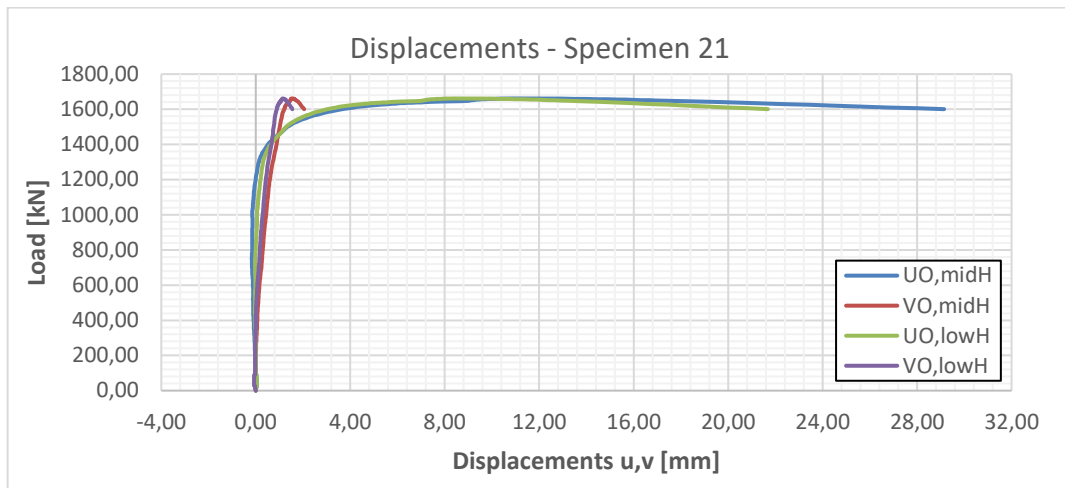


Figure B.26: Displacements of the corner point O along the principal axis, at mid-height and lower height (1/4H) cross-sections, for specimen 21

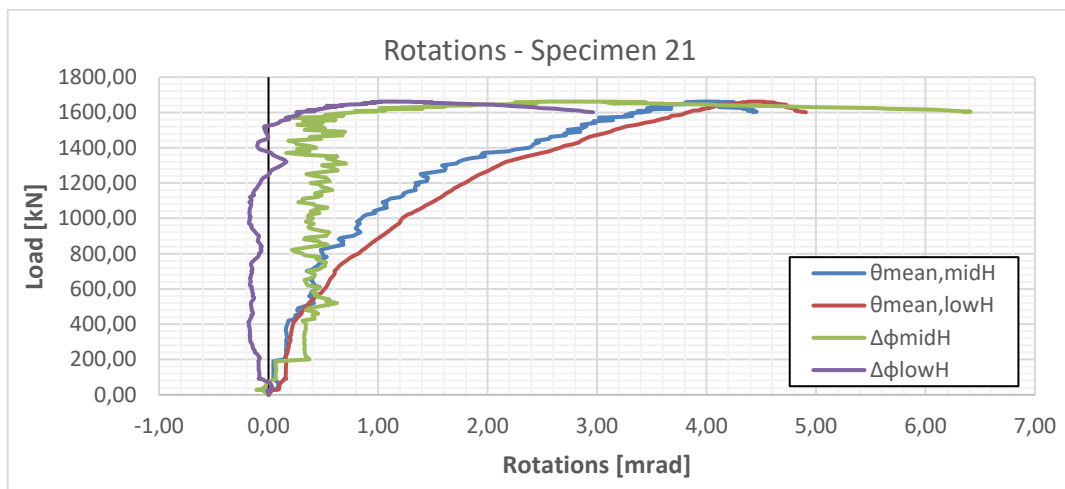


Figure B.27: Rotation along the length axe of two cross-sections along specimen 21

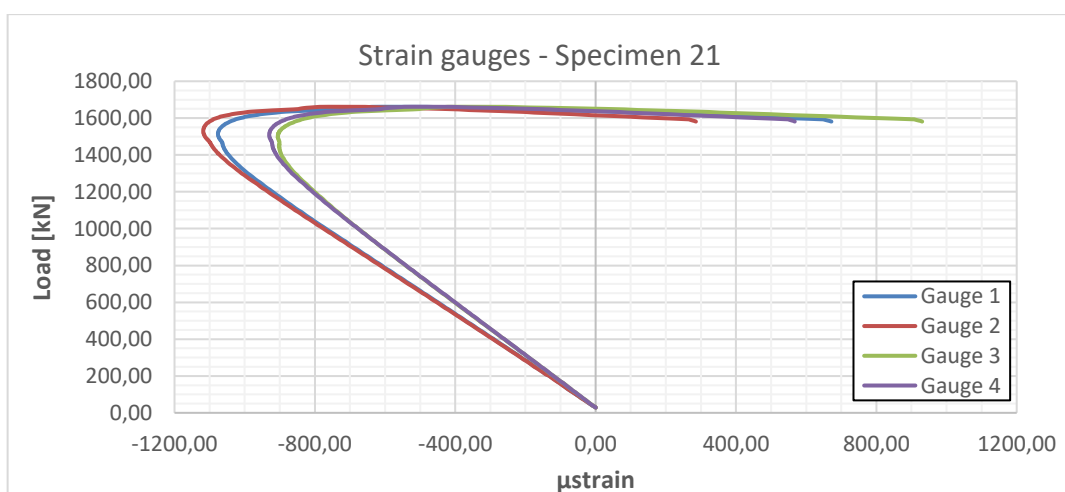
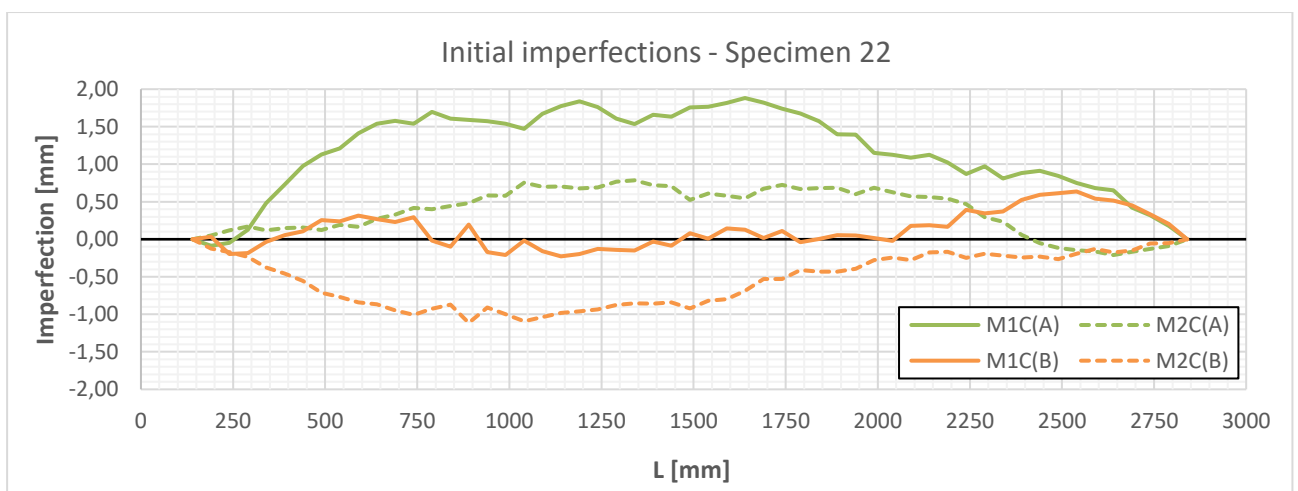


Figure B.28: Measurements of strain gauges on specimen 21

**B8. Specimen Sp22**

ID of specimen: Sp22	
Date of testing	20/05/2019
Type of test	Eccentrically loaded compression test
Mean actual dimensions	
Cross-section	L200x200x16
t <sub>1</sub> [mm]	16,39
t <sub>2</sub> [mm]	16,29
b <sub>1</sub> [mm]	200,36
b <sub>2</sub> [mm]	200,39
L [mm]	3000,00
L <sub>crit</sub> [mm]	3000+107=3107,00
Eccentricity e <sub>u</sub> [mm]	0,00
Eccentricity e <sub>v</sub> [mm]	66,64
Material	
Actual f <sub>y</sub> [Mpa]	487,6
Actual f <sub>u</sub> [Mpa]	604,6
Response	
Ultimate resistance [kN]	1341,35
Failure mode / Comments	Flexural-Torsional Buckling *A noise has been sounded from the weldings after the bulking



**Figure B.29: Initial imperfections of both faces along specimen 22**

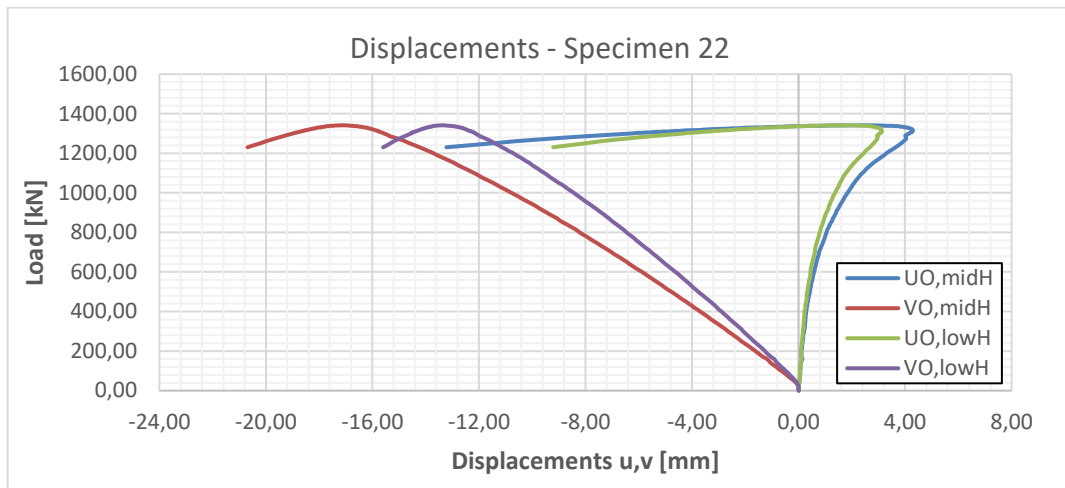


Figure B.30: Displacements of the corner point O along the principal axis, at mid-height and lower height (1/4H) cross-sections, for specimen 22

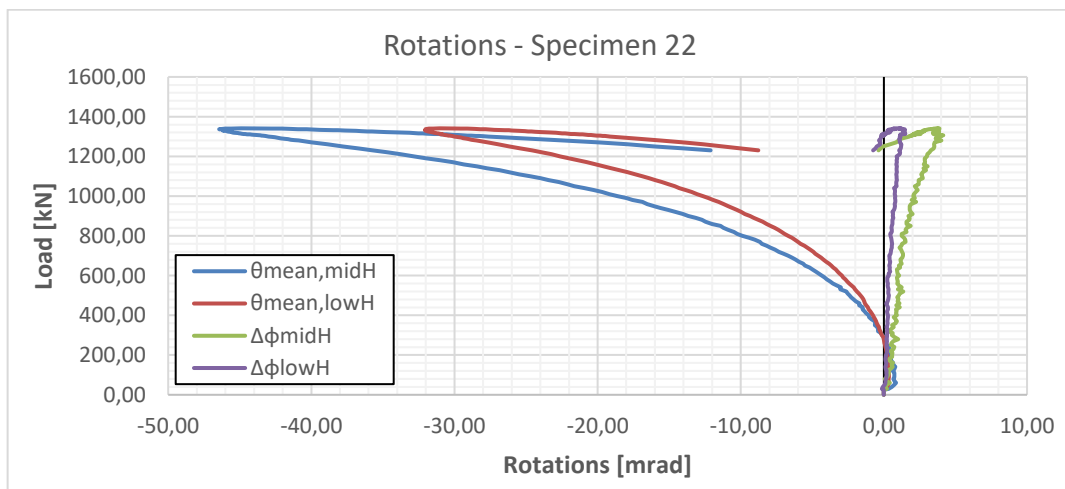


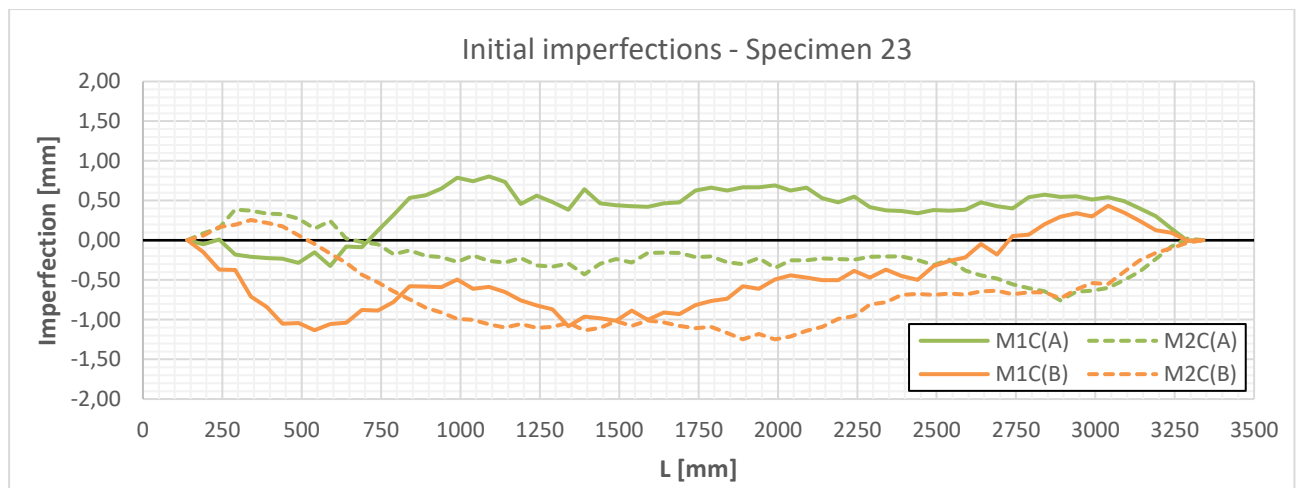
Figure B.31: Rotation along the length axis of two cross-sections along specimen 22



Figure B.32: Measurements of strain gauges on specimen 22

**B9. Specimen Sp23**

ID of specimen: Sp23	
Date of testing	17/05/2019
Type of test	Centrally loaded compression test
Mean actual dimensions	
Cross-section	L200x200x16
t <sub>1</sub> [mm]	16,32
t <sub>2</sub> [mm]	16,28
b <sub>1</sub> [mm]	200,25
b <sub>2</sub> [mm]	199,92
L [mm]	3500,00
L <sub>crit</sub> [mm]	3500+107=3607,00
Eccentricity e <sub>u</sub> [mm]	0,00
Eccentricity e <sub>v</sub> [mm]	0,00
Material	
Actual f <sub>y</sub> [Mpa]	487,6
Actual f <sub>u</sub> [Mpa]	604,6
Response	
Ultimate resistance [kN]	1227,96
Failure mode / Comments	Flexural Buckling



**Figure B.33: Initial imperfections of both faces along specimen 23**



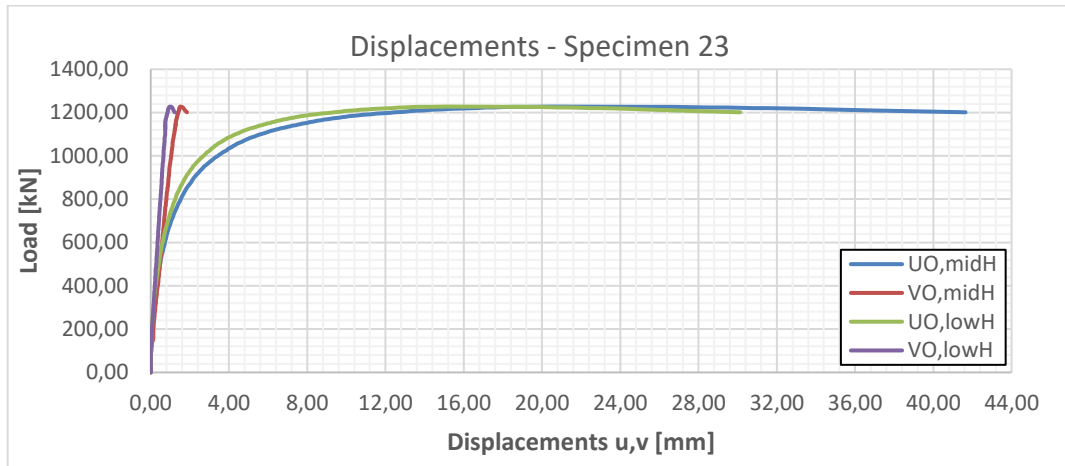


Figure B.34: Displacements of the corner point O along the principal axis, at mid-height and lower height (1/4H) cross-sections, for specimen 23

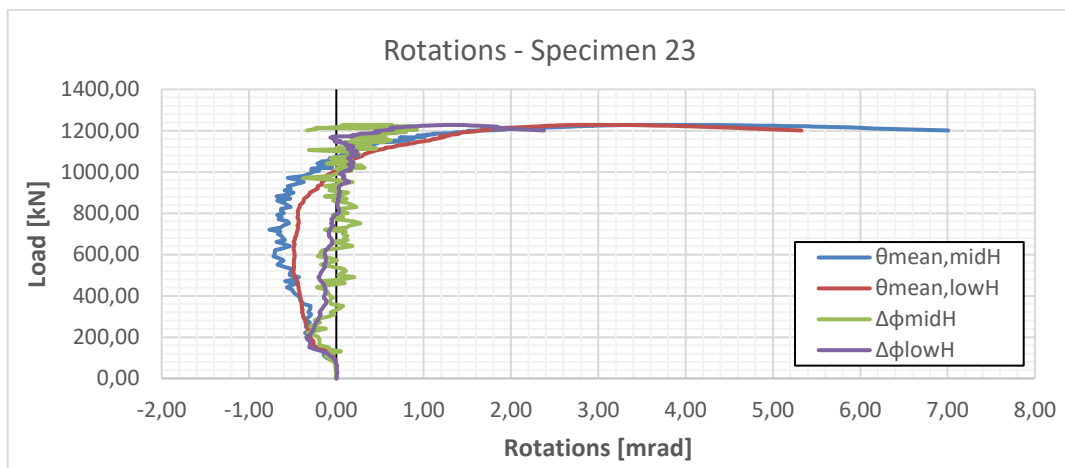


Figure B.35: Rotation along the length axis of two cross-sections along specimen 23

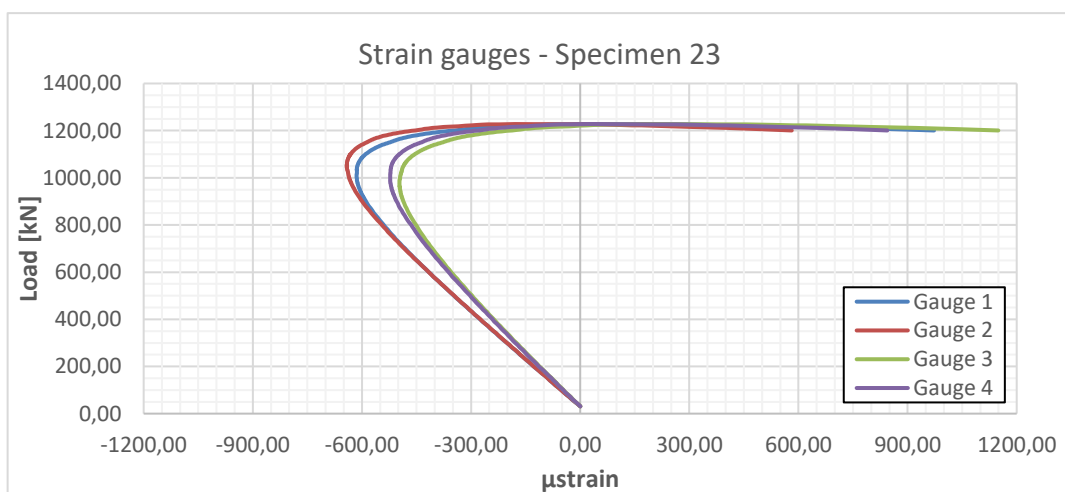

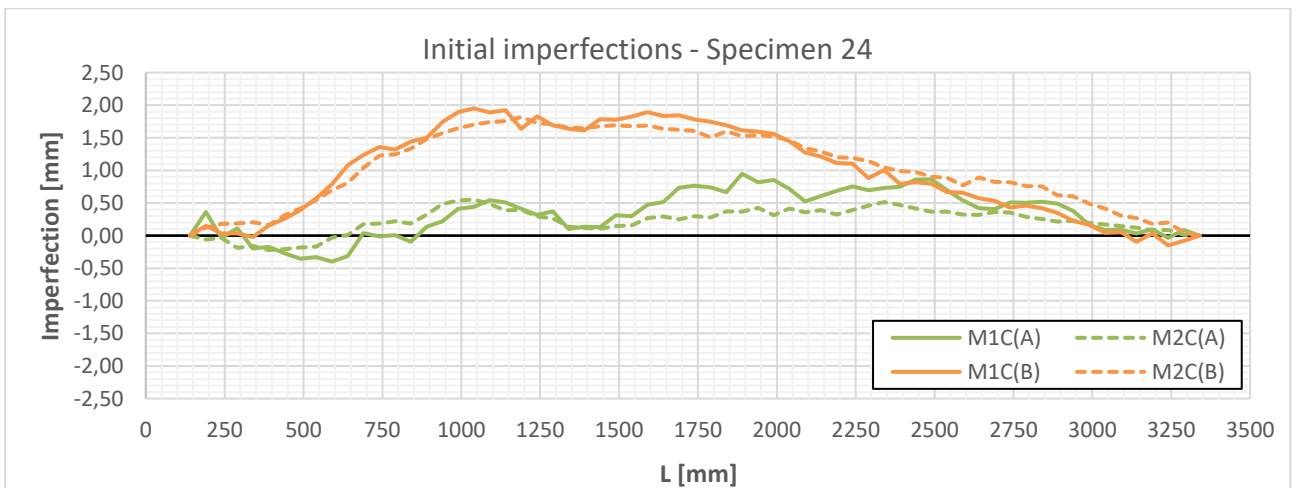


Figure B.36: Measurements of strain gauges on specimen 23

**B10. Specimen Sp24**

ID of specimen: Sp24	
Date of testing	24/10/2019
Type of test	Eccentrically loaded compression test
Mean actual dimensions	
Cross-section	L200x200x16
$t_1$ [mm]	16,42
$t_2$ [mm]	16,10
$b_1$ [mm]	200,05
$b_2$ [mm]	200,01
L [mm]	3500,00
$L_{crit}$ [mm]	$3500+107=3607,00$
Eccentricity $e_u$ [mm]	0,00
Eccentricity $e_v$ [mm]	66,64
Material	
Material	S 460/4
Actual $f_y$ [Mpa]	472,6
Actual $f_u$ [Mpa]	587,2
Response	
Ultimate resistance [kN]	1092,28
Failure mode / Comments	Flexural-Torsional Buckling

**Figure B.37: Initial imperfections of both faces along specimen 24**



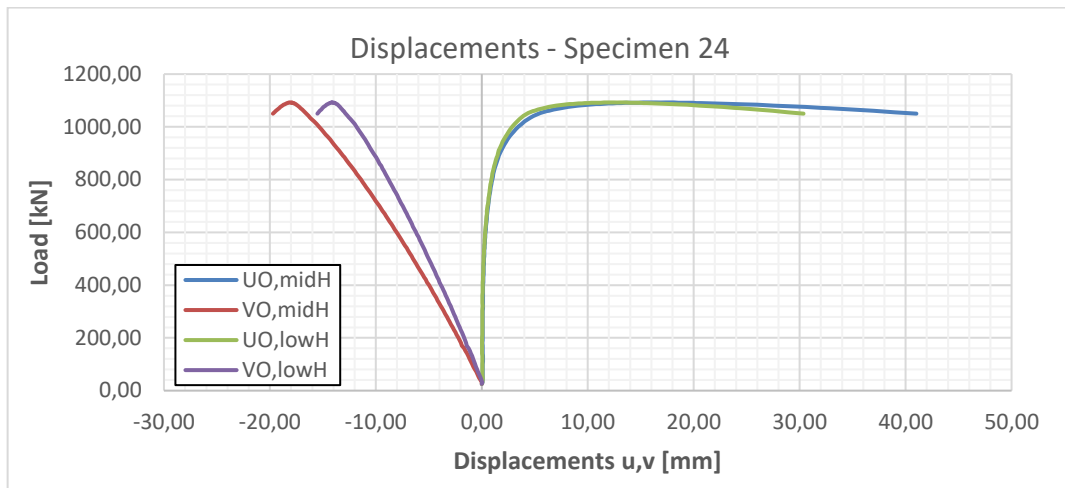


Figure B.38: Displacements of the corner point O along the principal axis, at mid-height and lower height (1/4H) cross-sections, for specimen 24

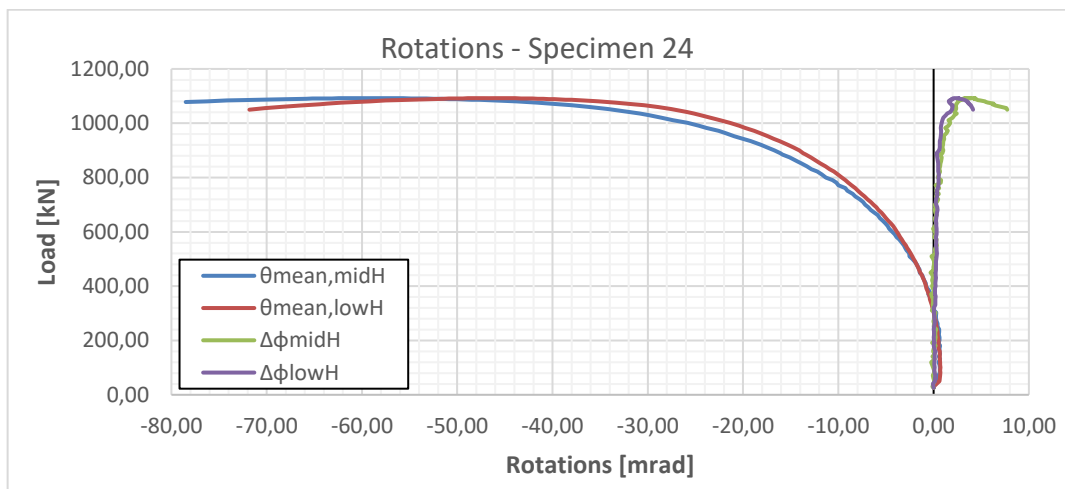


Figure B.39: Rotation along the length axe of two cross-sections along specimen 24

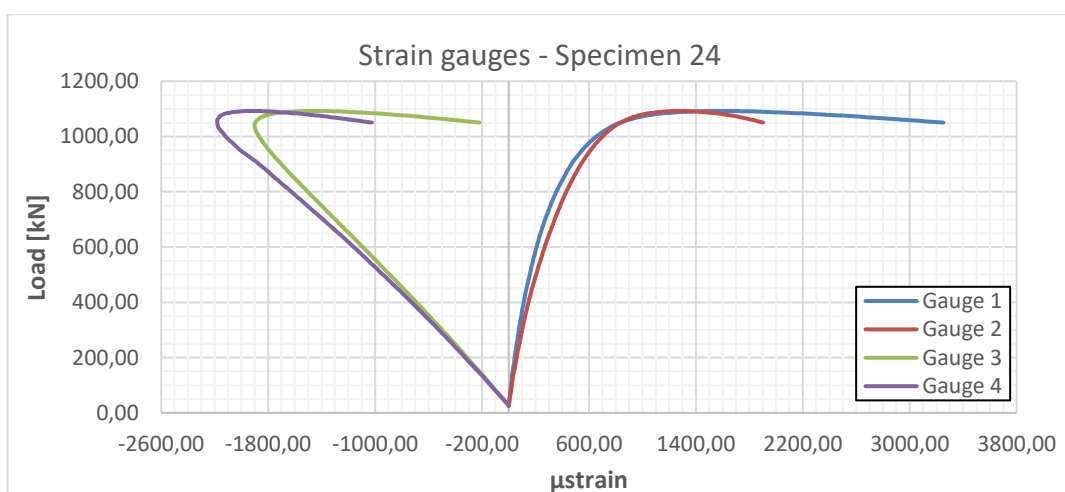
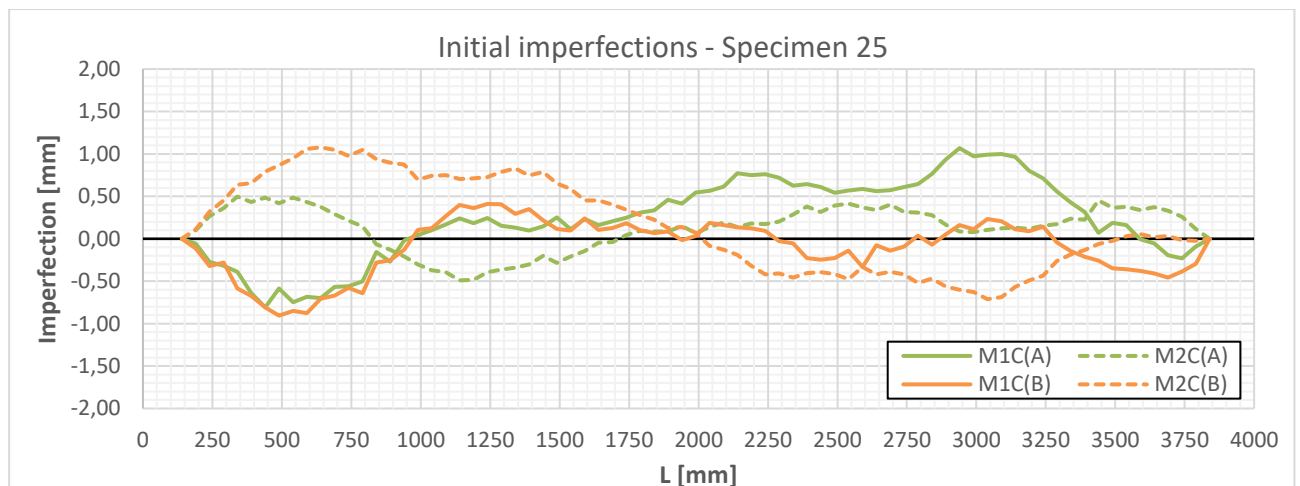


Figure B.40: Measurements of strain gauges on specimen 24

**B11. Specimen Sp25**

ID of specimen: Sp25	
Date of testing	21/05/2019
Type of test	Centrally loaded compression test
Mean actual dimensions	
Cross-section	L200x200x16
$t_1$ [mm]	16,33
$t_2$ [mm]	16,35
$b_1$ [mm]	199,96
$b_2$ [mm]	200,27
L [mm]	4000,00
$L_{crit}$ [mm]	$4000+107=4107,00$
Eccentricity $e_u$ [mm]	0,00
Eccentricity $e_v$ [mm]	0,00
Material	
Actual $f_y$ [Mpa]	487,6
Actual $f_u$ [Mpa]	604,6
Response	
Ultimate resistance [kN]	1048,07
Failure mode / Comments	Flexural Buckling



**Figure B.41: Initial imperfections of both faces along specimen 25**

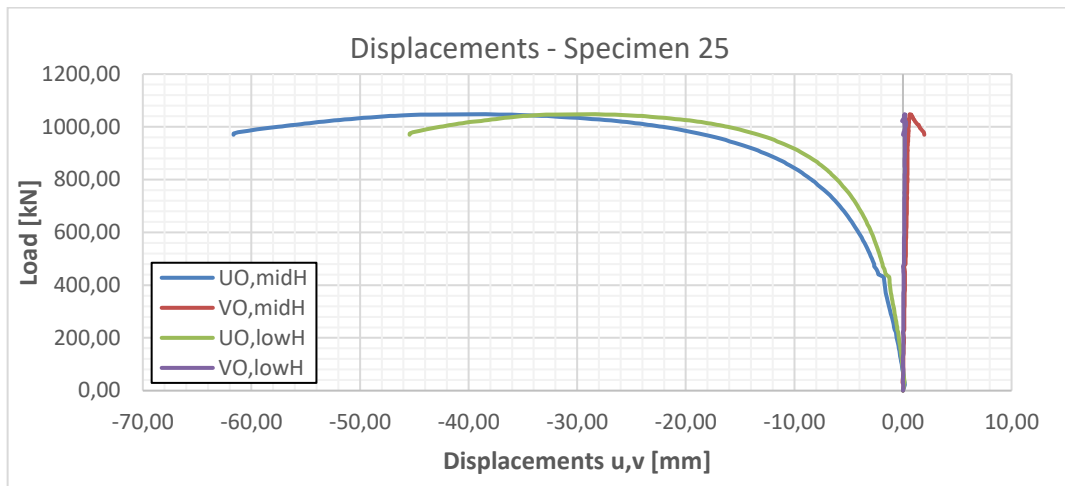


Figure B.42: Displacements of the corner point O along the principal axis, at mid-height and lower height (1/4H) cross-sections, for specimen 25

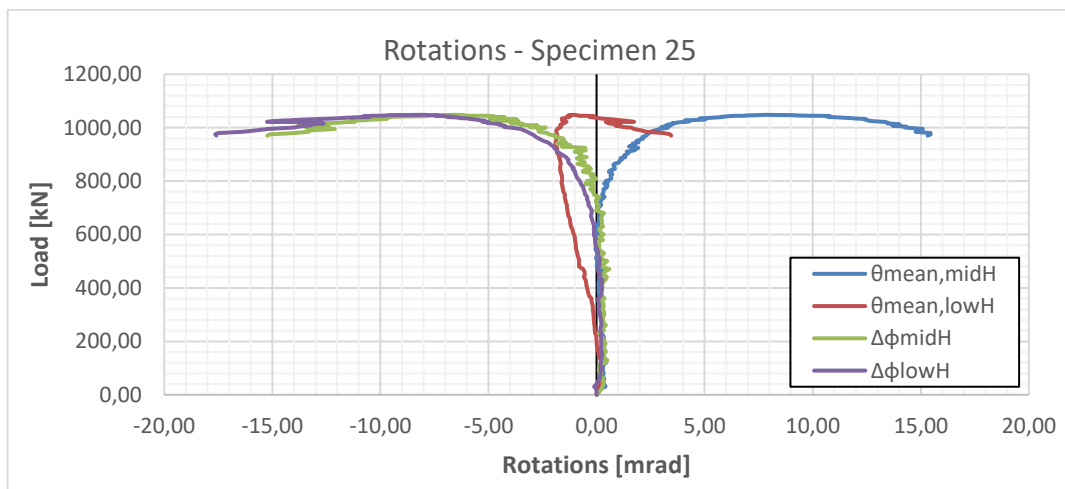


Figure B.43: Rotation along the length axe of two cross-sections along specimen 25

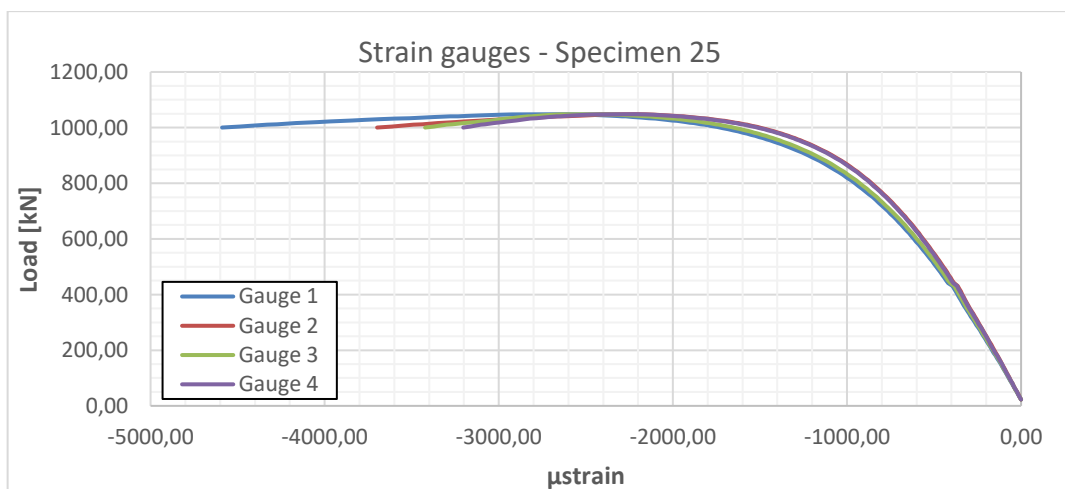

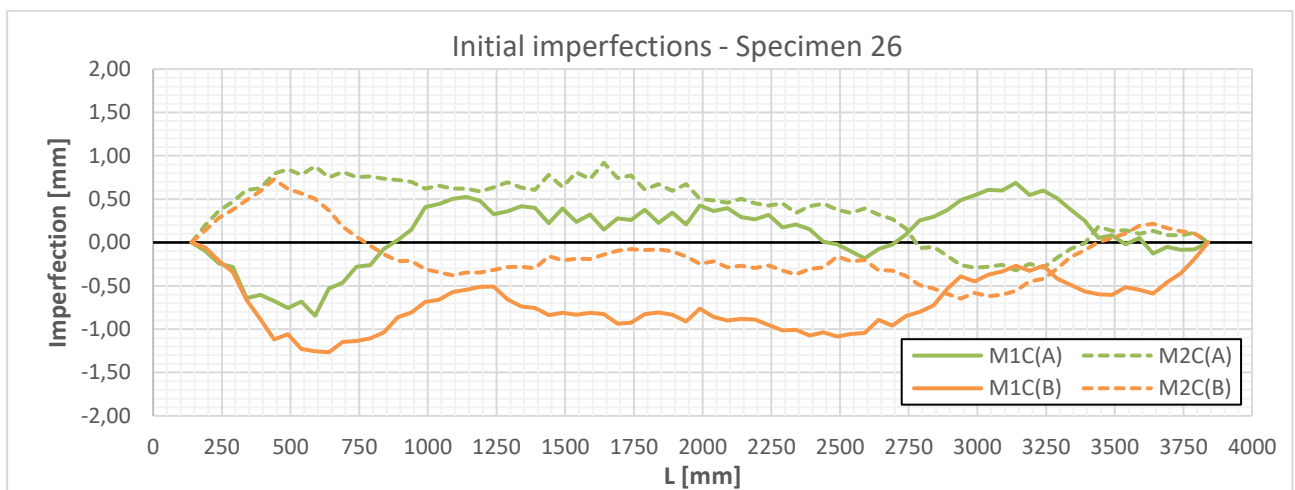


Figure B.44: Measurements of strain gauges on specimen 25

**B12. Specimen Sp26**

ID of specimen: Sp26	
Date of testing	22/05/2019
Type of test	Eccentrically loaded compression test
Mean actual dimensions	
Cross-section	L200x200x16
$t_1$ [mm]	16,32
$t_2$ [mm]	16,31
$b_1$ [mm]	200,06
$b_2$ [mm]	200,39
L [mm]	4000,00
$L_{crit}$ [mm]	$4000+107=4107,00$
Eccentricity $e_u$ [mm]	0,00
Eccentricity $e_v$ [mm]	66,64
Material	
Actual $f_y$ [Mpa]	487,6
Actual $f_u$ [Mpa]	604,6
Response	
Ultimate resistance [kN]	953,62
Failure mode / Comments	Flexural-Torsional Buckling

**Figure B.45: Initial imperfections of both faces along specimen 26**

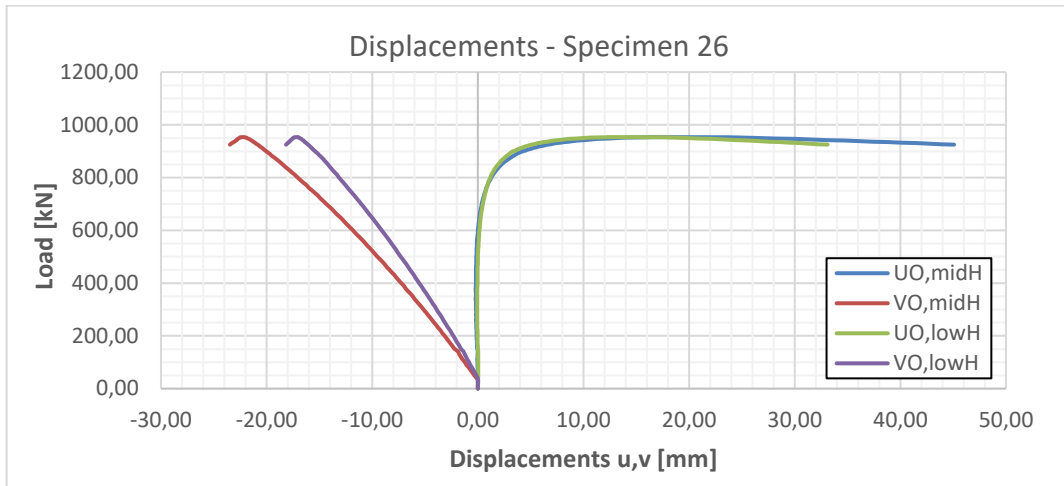


Figure B.46: Displacements of the corner point O along the principal axis, at mid-height and lower height (1/4H) cross-sections, for specimen 26

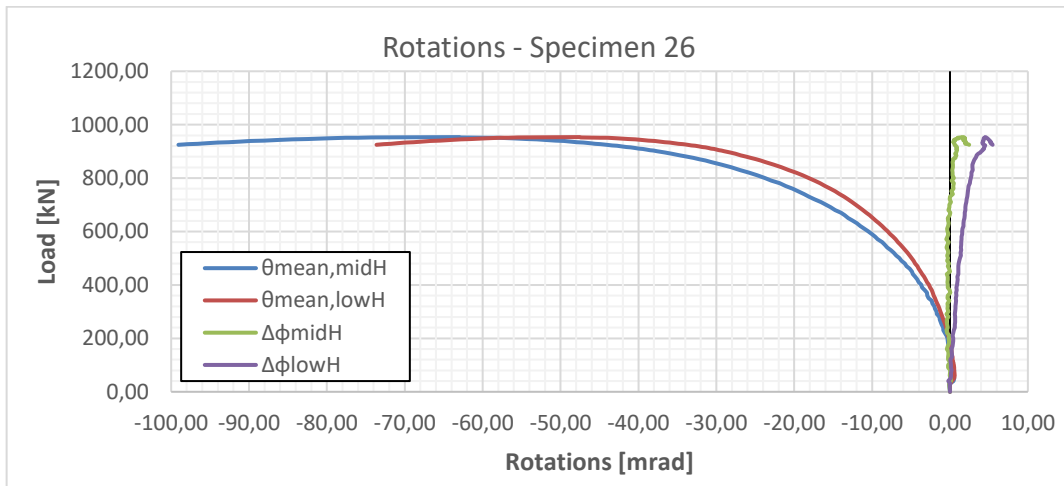


Figure B.47: Rotation along the length axe of two cross-sections along specimen 26

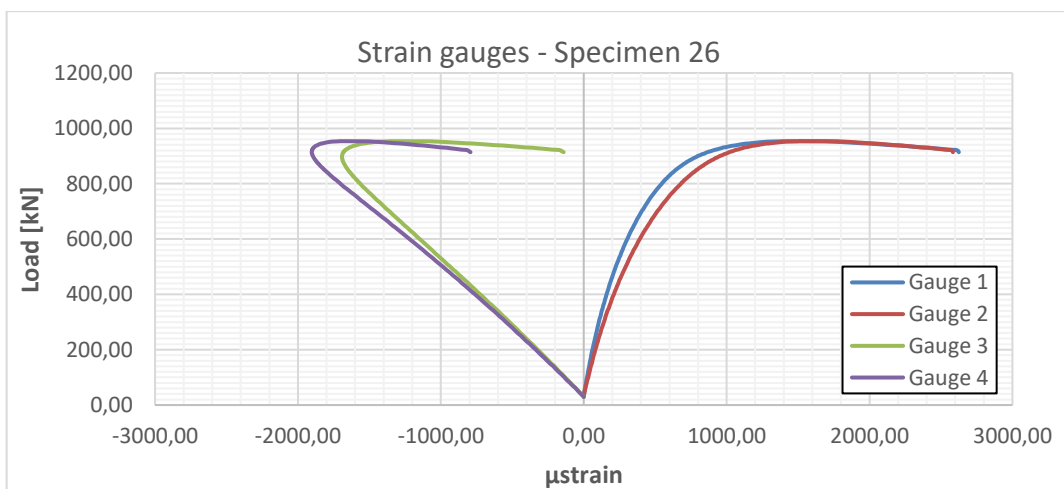


Figure B.48: Measurements of strain gauges on specimen 26